Finite-size DMRG characterization of the 1D spinless Fermi-Hubbard model phase diagram within the Bosonization framework

University of Pisa, a.y. 2024-2025

Alessandro Gori*

Final project for the Master's Degree course "Quantum Liquids"

Abstract

The one-dimensional spinless Fermi-Hubbard model at zero temperature is studied, employing finite-size DMRG algorithm to investigate some of its ground state properties. The model contains a hopping term between neighbouring sites, a finite on-site interaction energy, and a chemical potential. In order to investigate the zero-temperature ground-state properties of the model, finite-size DMRG was used.

The aim of the project is to observe a specific SU/CDW phase transition and explain it theoretically within the bosonization framework. In order to do so, the spinless Fermi-Hubbard model is bosonized and reduced to a renormalized Klein-Gordon field theory. Within this framework, the relevant parameters dominating the collective behavior are the renormalized velocity u and the Luttinger parameter K, which governs density-density and superconducting correlation functions. For a one-dimensional spinless model, bosonization allows for extraction of both parameters by computing second derivatives of ground-state energy at different setups. Finally, Jordan-Wigner technique is used to map the phase diagram onto the well-known XXZ phase diagram and reconnect the Mott insulating phases to spin Ferromagnetic/Anti-Ferromagnetic long-range orderings.

The entire project heavily relies upon the precedent project carried out by the author together with Marco Pompili, where the 1D Bose-Hubbard model was studied using finite-size DMRG. You may find at this link our previous work.

All of the code can be found at open-access in this repository:
`https://github.com/nepero27178/FermiHubbardDMRG`

Contents

*a.gori23@studenti.unipi.it / nepero27178@github.com

1 Theoretical introduction to bosonization

This first, vast section is devoted to the introduction of an extremely powerful technique in one-dimensional fermionic problems, namely, bosonization. It is widely based on the comprehensive work of Giamarchi, [3]. I won't get deep in the calculations neither in refined points about the method, being this last arbitrarily vast. The first part of this section deals with the spinless (a.k.a. polarized) case; the second part introduces the spin degree of freedom.

1.1 Bosonization in a nutshell for spinless fermions

The key idea is simple: start from a conventional fermionic-metallic hamiltonian,

$$\hat{H} = \hat{H}_0 + \hat{V} = \sum_k \xi_k \hat{c}_k^\dagger \hat{c}_k + \hat{V}$$

(I will leave the interaction unspecified, for a moment) where $\xi_k = \epsilon_k - \epsilon_F$ and I am using spinless fermions, for normal bands in ordinary fillings. Consider Fig. 1: the approximation in the above equation is exactly given by making the following assumption: since at low temperature (which, in metals, is a very broad definition) all the relevant Physics takes place at $\xi \sim 0$, and both the deep-down/far-away single-particle states do not contribute either due to Pauli pressure or state depletion, one can as well study the model:

$$\epsilon_k \to \left\{ \epsilon_k^{(\mathrm{L})}, \epsilon_k^{(\mathrm{R})} \right\}$$

Let s be the side index, $s \in \{\mathrm{L}, \mathrm{R}\}$, with

$$\mathrm{sgn}(s) = \begin{cases} +1 & \text{if} \quad s = \mathrm{R} \\ -1 & \text{if} \quad s = \mathrm{L} \end{cases}$$

Then I may approximate around the Fermi surface (in one dimension degenerated in two points)

$$\hat{H}_0 \simeq \hat{K}_0 \equiv \sum_{s \in \{\mathrm{L},\mathrm{R}\}} \sum_k \hbar v_F \left(\mathrm{sgn}(s) k - k_F \right) \left[\hat{c}_k^{(s)} \right]^\dagger \hat{c}_k^{(s)}$$

being $k_F \equiv \sqrt{2m\epsilon_F/\hbar}$ the Fermi wavevector and $v_F \equiv \hbar k_F / m$. $\hat{K}_0$ is the Tomonaga-Luttinger model. In the following, I will set $\hbar = 1$. Now, consider the side-wise density operators,

$$\hat{\rho}_q^{(s)} \equiv \sum_k \left[\hat{c}_{k+q}^{(s)} \right]^\dagger \hat{c}_k^{(s)}$$

Let me use a slightly different, somewhat lighter notation:

$$\hat{\rho}_q^{(s)} \leftrightarrow \hat{\rho}_s(q)$$

From now on, I will proceed only highlighting the important result in the bosonization procedure, since all the detailed derivation is included in [3].

1.1.1 Boson operators

The pivotal result in the bosonization technique is the following:

$$[\hat{\rho}_s(q), \hat{\rho}_{s'}(-q')] = -\delta_{ss'} \delta_{qq'} \mathrm{sgn}(s) \frac{qL}{2\pi} \tag{1}$$

where L is the one-dimensional system length. To get to this point, the very key passage is to employ the identity

$$\hat{A}\hat{B} =: \hat{A}\hat{B} : \; + \langle \Omega | \hat{A}\hat{B} | \Omega \rangle$$

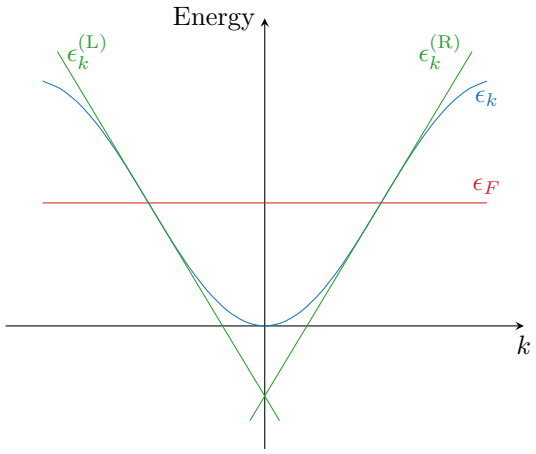

Figure 1 | Sketch of the fermionic band ϵ_k, the Fermi level ϵ_F and the two linear bands $\epsilon_k^{(\mathrm{L/R})}$ used to approximate the original bands around the Fermi surface. The double-linear model is often referred to as the Tomonaga-Luttinger model.

being $\hat{A}$, $\hat{B}$ two operators made of constructions/destructions, $|\Omega\rangle$ the generic many-body vacuum and $:\cdots:$ the normal ordering operation. Eq. (1) only holds if one uses this trick, which is, making a smart use of the infinite particle populations for the linearized model.

Now, Eq. (1) looks "bosonic". Notice that the left-side density operator vanishes identically for any $q > 0$ on the ground-state Fermi sea $|\Omega\rangle$. This is because it would require to destroy a fermion at any given k and creating one at $k + q$ – but the monotonicity of the linear left band prevents from doing so, because states on the left get deeper and deeper and thus are already occupied. In formulas

$$\hat{\rho}_{\mathrm{L}}(q > 0)\,|\Omega\rangle = 0$$
$$\hat{\rho}_{\mathrm{R}}(q < 0)\,|\Omega\rangle = 0$$

Then, I define a boson operator with finite particle numbers as

$$\hat{b}_q^\dagger \equiv \sqrt{\frac{2\pi}{|q|L}} \sum_{s\in\{\mathrm{L,R}\}} \mathrm{H}\left(\mathrm{sgn}(s)q\right) \hat{\rho}_s^\dagger(q)$$
$$\hat{b}_q \equiv \sqrt{\frac{2\pi}{|q|L}} \sum_{s\in\{\mathrm{L,R}\}} \mathrm{H}\left(\mathrm{sgn}(s)q\right) \hat{\rho}_s^\dagger(-q)$$

(here I define the Heaviside step function $\mathrm{H}(x)$) which of course satisfy

$$\left[\hat{b}_q, \hat{b}_{q'}^\dagger\right] = \delta_{qq'}$$

With a little patience, it can be shown that, taking $q \neq 0$,

$$\left[\hat{b}_q, \hat{K}_0\right] = v_F|q|\hat{b}_q \tag{2}$$

Assuming the (operatorial) basis generated by the bosonic operators to be complete, then this equation completely defines $\hat{K}_0$. It must hold:

$$\hat{K}_0 = \sum_{q\neq 0} v_F|q|\hat{b}_q^\dagger\hat{b}_q + (\text{a term for } q = 0)$$

This is astonishing result of the bosonization method: the kinetic term can be approximated by a quadratic free-bosons hamiltonian. Any quartic fermion interaction term (as are two-body interactions) is density-quadratic and can be cast to an identical form.

Fermionic-bosonic correspondence At the very heart of the bosonization technique, lies a change of basis in operators space: the hamiltonian is mapped from a fermionic representation to a bosonic one, limitedly to the energy regime of interest. In terms of the boson operators I shall express the fermion field operators,

$$\hat{\psi}_s(x) \equiv \frac{1}{\sqrt{L}} \sum_k e^{ikx} \hat{c}_k^{(s)}$$

which compose the total fermionic field just as

$$\hat{\psi}(x) = \hat{\psi}_{\mathrm{R}}(x) + \hat{\psi}_{\mathrm{L}}(x)$$

I also define a shifted version of the fermionic field, just by centering the momenta around the Fermi points. This amounts to

$$\hat{\psi}_s(x) \equiv e^{i\mathrm{sgn}(s)k_F x} \hat{\Psi}_s(s) \tag{3}$$

To derive the change of basis directly is non-trivial. However, it can be shown:

$$\left[\hat{\rho}_s^\dagger(q), \hat{\psi}_s(x)\right] = -e^{iqx} \hat{\psi}_s(x)$$

The above result is then used to extract the exact field representation in terms of density operators,

$$\hat{\psi}_s(x) = \hat{U}_s \exp\left\{ \mathrm{sgn}(s) \frac{2\pi}{L} \sum_q \frac{e^{iqx}}{q} \hat{\rho}_s(-q) \right\} \tag{4}$$

where $\hat{U}_s$ is a so-called Klein-Haldane factor. The operator $\hat{U}_s$ suppresses a charge uniformly, and is inserted by hand to make the fermion-boson mapping coherent and bijective.

1.1.2 Field-theoretic representation of the free hamiltonian

The final goal is to express the entire hamiltonian in terms of continuous bosonic fields. For now, define:

$$\hat{\phi}(x) \equiv -\colon \hat{N} \colon \frac{\pi x}{L} - \frac{i\pi}{L} \sum_{q\neq 0} \frac{e^{-\left(\frac{1}{2}\alpha|q| + iqx\right)}}{q} \sum_{s\in\{\mathrm{L,R}\}} \hat{\rho}_s^\dagger(q) \qquad (\alpha \to 0)$$

$$\hat{\theta}(x) \equiv \colon \Delta\hat{N} \colon \frac{\pi x}{L} + \frac{i\pi}{L} \sum_{q\neq 0} \frac{e^{-\left(\frac{1}{2}\alpha|q| + iqx\right)}}{q} \sum_{s\in\{\mathrm{L,R}\}} \mathrm{sgn}(s) \hat{\rho}_s^\dagger(q) \qquad (\alpha \to 0)$$

where $\hat{N} = \hat{N}^{(\mathrm{R})} + \hat{N}^{(\mathrm{L})}$, $\Delta\hat{N} = \hat{N}^{(\mathrm{R})} - \hat{N}^{(\mathrm{L})}$ and α is a convergence cutoff to regularize the theory. Notice that the side-wise number operators appear normal-ordered, thus have finite matrix elements. These field are defined like this for a reason: taking immediately the $\alpha \to 0$ limit and the x derivative,

$$\nabla\hat{\phi}(x) = -\pi \left[\hat{\rho}_{\mathrm{R}}(x) + \hat{\rho}_{\mathrm{L}}(x)\right] \qquad \nabla\hat{\theta}(x) = \pi \left[\hat{\rho}_{\mathrm{R}}(x) - \hat{\rho}_{\mathrm{L}}(x)\right] \tag{5}$$

being the spatial density simply given by Fourier-transforming our q-wise density,

$$\hat{\rho}(x) = \frac{1}{L} \sum_q e^{-iqx} \hat{\rho}(q) = \frac{1}{L} \sum_q e^{-iqx} \sum_{s\in\{\mathrm{L,R}\}} \hat{\rho}_s(q)$$

Here, the second "=" sign is the passage where I actively switched to the Tomonaga-Luttinger model of Fig. 1. Then:

$$-\frac{\nabla\hat{\phi}(x)}{\pi} \quad \to \quad \text{particle density, "canonical position"}$$
$$\frac{\nabla\hat{\theta}(x)}{\pi} \quad \to \quad \text{particle RL unbalance, "canonical momentum"}$$

Object	Density expression
Fermionic field	$\hat{\psi}_s(x) = \hat{U}_s \exp\left\{ \mathrm{sgn}(s) \frac{2\pi}{L} \sum_q \frac{e^{iqx}}{q} \hat{\rho}_s(-q) \right\}$
Boson operator	$\hat{b}_q = \sqrt{\frac{2\pi}{\lvert q \rvert L}} \sum_{s \in \{\mathrm{L,R}\}} \theta\left(\mathrm{sgn}(s) q\right) \hat{\rho}_s^\dagger(-q)$
Boson fields gradients	$\nabla\hat{\phi}(x) = -\pi\left[\hat{\rho}_\mathrm{R}(x) + \hat{\rho}_\mathrm{L}(x)\right]$ $\nabla\hat{\theta}(x) = \pi\left[\hat{\rho}_\mathrm{R}(x) - \hat{\rho}_\mathrm{L}(x)\right]$

Table 1 | Summary of the relevant quantities of the bosonization scheme as expressions involving physical (side resolved) fermionic density.

The difference $\hat{\rho}_\mathrm{R} - \hat{\rho}_\mathrm{L}$ is related to the current operator in one dimension: it just subtracts, point-wise, the left-going density from the right-going density.

For the sake of completeness, here I also report the expression for the fermionic fields in term of the bosonic ones:

$$\hat{\psi}_s(x) = \frac{\hat{U}_s}{\sqrt{2\pi\alpha}} \exp\left\{ i\left(\mathrm{sgn}(s) k_F - \frac{\pi}{L}\right) x - i\left(\mathrm{sgn}(s)\hat{\phi}(x) + \hat{\theta}(x)\right)\right\} \qquad (\alpha \to 0) \tag{6}$$

This expression is valid in the thermodynamic limit. Let me go straight to the end: expressing the above fields in terms of boson operators it turns out that

$$\left[\hat{\phi}(x), \frac{\nabla\hat{\theta}(y)}{\pi}\right] = i\delta(x-y)$$

Thus, the fields $\hat{\phi}(x)$ and $\hat{\Pi}(x) \equiv \nabla\hat{\phi}(x)/\pi$ are bosonic and canonically conjugate. Skipping some passages the reader can find in [3, Chap. 2], the hamiltonian is represented in field language as:

$$\hat{H}_0 \simeq \hat{K}_0 = \frac{1}{2\pi} \int_0^L dx\, v_F \left[\left(\nabla\hat{\phi}(x)\right)^2 + \left(\nabla\hat{\theta}(x)\right)^2\right] \tag{7}$$

This is the very cornerstone of bosonization. This is the Klein-Gordon bosonic-massless hamiltonian. Apart from pure math, what we obtained is a consequence of the strict one-dimensional topology: in such low dimensionality the Fermi surface reduces to two points ($k = \pm k_F$), thus the only low-energy particle-hole excitations allowed (those collective excitations proper of a system of free fermions) either have a well defined momentum of $q \simeq 0$ or $q \simeq \pm 2k_F$. Low energy spectrum only exists strictly around these points.

Particle-hole excitations are always made of a combined creation and annihilation of fermions, thus intuitively remind of a "bosonic character". In order to interpret such excitations as bosons, however, they must be somewhat stable. This only happens in one dimension: here, particle-hole excitations *are* emergent bosons. I won't enter in deep details here, recalling the main reference of this report [3] and its exceptional cover of the topic. To make the discussion here clearer, however, it must be cited that the reason for insurgence of boson fields is the fact that the use of a linear spectrum ensures independence of the particle-hole spectrum from the starting point on the (degenerated) Fermi surface, and thus makes the fermion-to-boson mapping possible.

As a final remark, notice that combining Eqns. (7) and (5), the above hamiltonian reduces to

$$\hat{K}_0 = \pi \int_0^L dx\, v_F \left[\hat{\rho}_\mathrm{R}^2(x) + \hat{\rho}_\mathrm{L}^2(x)\right] \tag{8}$$

a rewriting that will become useful later on. A prefactor $\hbar$ on the right side is to be reintroduced to be dimensionally correct.

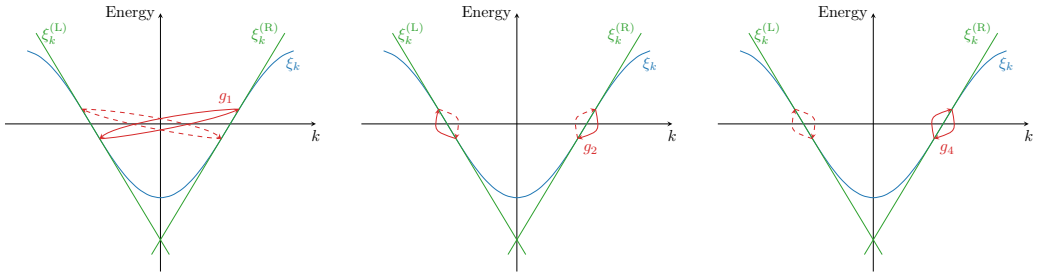

a | $g_1 = V(q \approx \pm 2k_F)$ process. b | $g_2 = V(q \approx 0)$ process. c | $g_4 = V(q \approx 0)$ process.

Figure 2 | Diagrammatic sketch of the possible two-fermions interaction in the spinless scenario.

1.1.3 Inserting interactions

It is time to let in interactions. As said, particle-hole excitations exchange a fermion from the Fermi sea with a hole from outside. Due to the strict topology of the Fermi surface, only three processes actually contribute – namely g_1, g_2 and g_4, respectively in Figs. 2a-2b-2c. Note that, for spinless fermions, due to particles indistinguishability, actually g_1 and g_2 are the same process[1].

Now, consider a particle-hole symmetric interaction, *quartic* in the fermionic operators,

$$V \sim c^\dagger c^\dagger c c$$

as is for instance an s-wise spatial density-density interaction,

$$\hat{V} = \sum_{s_1 \in \{\mathrm{L,R}\}} \sum_{s_2 \in \{\mathrm{L,R}\}} \int_0^L dx_1 \int_0^L dx_2 \, V_{s_1 s_2}(x_1 - x_2) \hat{\rho}_{s_1}(x_1) \hat{\rho}_{s_2}(x_2)$$

coupling left-going and right-going fermions. I collect g_4 processes as those terms with $s_1 = s_2$ and g_1, g_2 processes as those terms with $s_1 \neq s_2$,

$$\underbrace{\hat{\rho}_{\mathrm{R}}(x_1)\hat{\rho}_{\mathrm{R}}(x_2) \quad \hat{\rho}_{\mathrm{L}}(x_1)\hat{\rho}_{\mathrm{L}}(x_2)}_{g_4} \qquad \underbrace{\hat{\rho}_{\mathrm{R}}(x_1)\hat{\rho}_{\mathrm{L}}(x_2) \quad \hat{\rho}_{\mathrm{L}}(x_1)\hat{\rho}_{\mathrm{R}}(x_2)}_{g_1 = g_2}}$$

At this point, I make an apparently heavy assumption. Let me use for now a contact-like interaction[2],

$$[V(x-y)] = \frac{1}{2} \begin{bmatrix} g_4 & g_2 \\ g_2 & g_4 \end{bmatrix} \delta(x-y) \qquad \text{with } g_2, g_4 \in \mathbb{R}$$

(with a little notation abuse, I used the side indices s_1, s_2 as row-column indices). Let me analyze separately the contributions to the hamiltonian: $\hat{V} = \hat{V}_2 + \hat{V}_4$.

g_4 process. This is the simpler case. The densities vertex contributions to $\hat{K}_0$ is simply

$$\hat{V}_4 = \frac{1}{2} g_4 \int_0^L dx \, [\hat{\rho}_{\mathrm{R}}(x)\hat{\rho}_{\mathrm{R}}(x) + \hat{\rho}_{\mathrm{L}}(x)\hat{\rho}_{\mathrm{L}}(x)]$$

Recalling Eq. (5),

$$\begin{aligned} \hat{V}_4 &= g_4 \int_0^L dx \left[\left(\frac{\nabla\hat{\phi}(x) - \nabla\hat{\theta}(x)}{2\pi} \right)^2 + \left(\frac{\nabla\hat{\phi}(x) + \nabla\hat{\theta}(x)}{2\pi} \right)^2 \right] \\ &= \frac{g_4}{2\pi v_F} \times \frac{1}{2\pi} \int_0^L dx \, v_F \left[\left(\nabla\hat{\phi}(x) \right)^2 + \left(\nabla\hat{\theta}(x) \right)^2 \right] \\ &= \frac{g_4}{2\pi v_F} \hat{K}_0 \end{aligned}$$

[1] I here skip an explanation about how to absorb g_1 inside g_2, a detail that becomes clear in the spinful case.

[2] For the type of interaction I will consider in this project, which is a NN neighbors interaction onto a closed chain, this assumption actually makes sense in thermodynamic limit.

which is remarkable: considering this process, the hamiltonian looks like:

$$\hat{K}_0 + \hat{V}_4 + \hat{V}_2 = \frac{1}{2\pi}\int_0^L dx \underbrace{v_F\left(1+\frac{g_4}{2\pi v_F}\right)}_{u}\left[\left(\nabla\hat{\phi}(x)\right)^2 + \left(\nabla\hat{\theta}(x)\right)^2\right] + \hat{V}_2$$

Now, u is the bosons velocity renormalized by g_4-like interactions.

g_2 **process.** In a very similar fashion, it is easy to obtain

$$\begin{aligned}\hat{V}_2 &= \frac{1}{2}g_2\int_0^L dx\left[2\left(\frac{\nabla\hat{\phi}(x)-\nabla\hat{\theta}(x)}{2\pi}\right)\left(\frac{\nabla\hat{\phi}(x)+\nabla\hat{\theta}(x)}{2\pi}\right)\right]\\ &= \frac{g_2}{2\pi v_F}\cdot\frac{1}{2\pi}\int_0^L dx\, v_F\left[\left(\nabla\hat{\phi}(x)\right)^2 - \left(\nabla\hat{\theta}(x)\right)^2\right]\end{aligned}$$

It is not so immediate to insert this term in the interacting hamiltonian. However, an elegant formulation exists involving two parameters u and K:

$$\hat{K}_0 + \hat{V}_4 + \hat{V}_2 = \frac{1}{2\pi}\int_0^L dx\left[\frac{u}{K}\left(\nabla\hat{\phi}(x)\right)^2 + uK\left(\nabla\hat{\theta}(x)\right)^2\right] \tag{9}$$

trivially defined as

$$\frac{u}{K} \equiv 1 + \frac{g_4}{2\pi v_F} + \frac{g_2}{2\pi v_F} \qquad uK \equiv 1 + \frac{g_4}{2\pi v_F} - \frac{g_2}{2\pi v_F}$$

a condition simultaneously satisfied by

$$u = v_F\sqrt{\left(1+\frac{y_4}{2}\right)^2 - \left(\frac{y_2}{2}\right)^2} \qquad K = \sqrt{\frac{2+y_4-y_2}{2+y_4+y_2}} \qquad y_i \equiv \frac{g_i}{\pi v_F}$$

This collection of equation is everything one needs to completely map a one-dimensional interacting fermionic problem into a renormalized free bosonic problem. Everything I have done hold for spinless fermions and contact interaction, but can be extended.

1.1.4 The euclidean action

I here briefly sketch the derivation of the bosonized euclidean action. Starting from the hamiltonian density,

$$\hat{\mathcal{K}}[\phi,\Pi] = \frac{1}{2\pi}\left[\frac{u}{K}\left(\nabla\hat{\phi}(x)\right)^2 + uK\left(\pi\hat{\Pi}(x)\right)^2\right]$$

the euclidean action is immediately recovered by Legendre-transforming $\hat{\mathcal{K}}$ in imaginary time,

$$\begin{aligned}\mathcal{L}[\phi,\Pi] &= i\Pi\frac{\partial}{\partial\tau}\phi - \mathcal{K}[\phi,\Pi]\\ &= \frac{1}{2\pi}\left[2i\nabla\theta\frac{\partial}{\partial\tau}\phi - \frac{u}{K}\left(\nabla\phi\right)^2 + uK\left(\nabla\theta\right)^2\right]\end{aligned}$$

Now the calculation gets a little intricate, and I will skip it. The key point is to recognize that, being L the lagrangian,

$$S[\phi,\Pi] \equiv \int_0^\beta d\tau\, L[\phi,\Pi] = \int_0^\beta d\tau\int_0^L dx\,\mathcal{L}[\phi,\Pi]$$

and $\mathcal{Z}$ the partition function

$$\mathcal{Z} \equiv \int \mathcal{D}[\phi]\mathcal{D}[\Pi]e^{-S[\phi,\Pi]/\hbar}$$

one is able to complete the square for the $\nabla\theta$ part appearing in $\mathcal{L}$ and reduce the Π part of the above integral to a gaussian form. The same trick holds for any Π-independent observable we may want to average. The final, effective ϕ-action is just

$$S_\phi \equiv \frac{1}{2\pi}\int_0^\beta d\tau \int_0^L dx \left[\frac{1}{uK}\left(\partial_\tau\phi(x,\tau)\right)^2 + \frac{u}{K}\left(\nabla\phi(x,\tau)\right)^2\right] \tag{10}$$

which, exponentiated, is the path integral statistical weight.

1.2 Spinless fermions observables

The big, heavy (but wondrous) theoretical part is over: let's get operative. My aim is to estimate the renormalized parameters u and K. First, it must be understood how to get them out of some observables.

1.2.1 Charge compressibility

A very simple observable, usable for estimating easily the ratio u/K, is charge compressibility. Let μ be the chemical potential,

$$\hat{K} \to \hat{K} - \mu\int_0^L dx\,\hat{\rho}(x)$$

Following the convention of Giamarchi, I will define compressibility as

$$\kappa \equiv \frac{\partial\rho}{\partial\mu} \qquad \rho = \frac{1}{L}\int_0^L dx\,\langle\hat{\rho}(x)\rangle$$

(notice that usually the definition above is completed by a prefactor ρ^{-2}, I omit). Using Eq. (5)[3],

$$\begin{aligned}\frac{\partial\rho}{\partial\mu} &= \frac{\partial}{\partial\mu}\frac{1}{L}\int_0^L dx\,\langle\hat{\rho}(x)\rangle \\ &= -\frac{1}{\pi L}\frac{\partial}{\partial\mu}\int_0^L dx\,\left\langle\nabla\hat{\phi}(x)\right\rangle\end{aligned}$$

Now, consider the term I am adding to the hamiltonian: let me add a pure energy shift term (physically irrelevant) and manipulate the above expression a bit,

$$\begin{aligned}-\mu\int_0^L dx\,\hat{\rho}(x) &= \frac{\mu}{\pi}\int_0^L dx\,\nabla\hat{\phi}(x) + \Delta \\ &= \frac{1}{2\pi}\times 2\int_0^L dx\,\frac{u}{K}\left(\mu\frac{K}{u}\right)\left(\nabla\hat{\phi}(x)\right) + \underbrace{\frac{1}{2\pi}\int_0^L dx\,\left(\mu\frac{K}{u}\right)^2}_{\Delta}\end{aligned}$$

It is now immediate to see that if I define

$$\hat{\varphi}(x) \equiv \hat{\phi}(x) + \mu\frac{K}{u}x$$

we have:

$$\hat{K} - \mu\int_0^L dx\,\hat{\rho}(x) = \frac{1}{2\pi}\int_0^L dx\left[\frac{u}{K}\left(\nabla\hat{\varphi}(x)\right)^2 + uK\left(\nabla\hat{\theta}(x)\right)^2\right]$$

an expression canonically equivalent to Eq. (9). Now, for this new system the term $\nabla\hat{\varphi}$ represents charge density fluctuations. This implies that $\langle\nabla\hat{\varphi}\rangle = 0$ at any point. Then,

$$-\left\langle\nabla\hat{\phi}(x)\right\rangle = \mu\frac{K}{u}$$

[3]To be complete, I here am hiding a passage. In fact, $\pi\hat{\rho} = \pi\left[\mathrm{RR}+\mathrm{LL}+\mathrm{RL}+\mathrm{LR}\right]$ (here I use the shorthand notation $\mathrm{s_1s_2} = \hat{\psi}^\dagger_{s_1}\hat{\psi}_{s_2}$). Taking the average value, $\pi\langle\hat{\rho}\rangle = \pi\langle\mathrm{RR}+\mathrm{LL}\rangle + \pi\langle\mathrm{RL}+\mathrm{LR}\rangle$, and it's evident by symmetry that $\langle\mathrm{RL}+\mathrm{LR}\rangle = 0$; which justifies the last line, since $\pi\langle\mathrm{RR}+\mathrm{LL}\rangle = -\langle\nabla\hat{\phi}\rangle$.

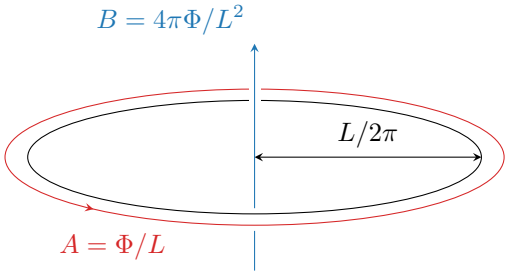

Figure 3 | Schematics of a static flux Φ pinning through a ring of circumference L.

Finally:

$$\begin{aligned}\frac{\partial\rho}{\partial\mu} &= -\frac{1}{\pi L}\frac{\partial}{\partial\mu}\int_0^L dx\,\left\langle\nabla\hat{\phi}(x)\right\rangle \\ &= \frac{\partial}{\partial\mu}\mu\frac{K}{\pi u}\times\frac{1}{L}\int_0^L dx = \frac{K}{\pi u}\end{aligned} \tag{11}$$

Then, to measure the ratio u/K I need to measure the quantity $(\pi\Delta\rho/\Delta\mu)^{-1}$ (times $\hbar$, to be dimensionally correct). This most certainly is a simple quantity to be measured by the means of a DMRG simulation.

1.2.2 Charge stiffness

Another observable rather easy to compute numerically is the charge stiffness; which is basically the tendency of the system to respond to an external charge-coupling field. Now, assuming a closed-chain topology (as in Fig. 3), a flux Φ threading the ring accounts for a static vector potential

$$A = \frac{\Phi}{L}$$

I define the unit flux as: $\Phi_0 \equiv h/e$. The overall effect on the fermionic system is an overall momentum shift originated by the covariant derivative formulation,

$$k \to k - \frac{e}{\hbar}A = k - \frac{2\pi}{L}\frac{\Phi}{\Phi_0}$$

Let me define the shift angle:

$$\eta \equiv 2\pi\frac{\Phi}{\Phi_0}$$

Finally, absorbing the latter as a gauge transformation, this translates in the presence of twisted boundary conditions by an angle $2\pi\Phi/\Phi_0$ in the wavefunction. Now, given the band $\xi_k[\Phi]$, the current density is simply

$$\begin{aligned}J &= \frac{1}{L}\sum_{k:\,\xi_k\leq 0}\frac{1}{\hbar}\frac{\partial}{\partial k}\xi_k[\Phi]\Big|_\Phi \\ &= J_0 + \frac{1}{L\hbar}\sum_{k:\,\xi_k\leq 0}L\frac{\partial}{\partial\eta}\xi_k[\Phi]\Big|_\Phi \\ &= \frac{1}{\hbar}\frac{\partial}{\partial\eta}E[\Phi]\end{aligned}$$

In the second passage I have isolated the contribution to the derivative given from the free system J_0, null by symmetry, and in the last the ground-state energy $E[\Phi]$ was recognized as the sum of all single-particle occupied states.

Now, charge stiffness is simply the zero-flux current response:

$$\mathcal{D} = \frac{\partial J}{\partial\Phi}\Big|_{\Phi=0}$$

As for the compressibility, I adopt a slightly different (and charge-neutral) definition,

$$\mathcal{D} \equiv \frac{\pi L}{e} \frac{\partial J}{\partial \Phi}\bigg|_{\Phi=0} \tag{12}$$

Inserting the previous result,

$$\mathcal{D} = \frac{\pi L}{e} \frac{\Phi_0}{2\pi} \frac{\partial J}{\partial \eta}\bigg|_{\Phi=0} = \pi L \frac{\partial^2}{\partial \eta^2} E[\Phi]\bigg|_{\Phi=0}$$

The second derivative of the ground-state energy, taken with respect to the twisting angle, is – apart from some factors – the charge stiffness.

I now need to link all of this with the bosonization scheme. The procedure is identical to the one carried out for the charge compressibility in last paragraph:

1. Include the minimally coupled interaction in the euclidean effective action of Eq. (10),

$$S_\phi \to S_\phi - \int dx\, J(x) A(x) = S_\phi - \frac{\Phi}{L} \int dx\, J(x)$$

2. The charge density current in one dimension is obtained easily from the continuity equation:

$$\partial_t \rho + \nabla j = 0 \qquad \Longrightarrow \qquad j = \frac{1}{\pi} \partial_t \phi$$

   having used $\rho = -\nabla\phi/\pi$ and ignored boundary terms.

3. A constant added to the action does not change its variational properties. Thus, defining

$$\varphi \equiv \phi - uK \frac{\Phi}{L} \tau$$

   neither the time nor the spatial part get affected by the transformation, and the action for a flux-free system is recovered.

4. Since for the flux-free system the induced current is zero,

$$J = \frac{1}{\pi} \langle \partial_\tau \phi \rangle = uK \frac{\Phi}{\pi L}$$

Recalling the definition of $\mathcal{D}$ of Eq. (12), finally

$$\mathcal{D} = uK \tag{13}$$

which is the second relation I needed in order to determine u and K. The entirety of this derivation could have been worked out analogously by expressing the current in terms of the conjugate momentum field Π and completing the square directly in the hamiltonian.

Equal-time Green's function

The single-particle Green's function is defined in imaginary time, and for s-side fermions, as:

$$\mathcal{G}_s(x,\tau) \equiv -\left\langle \mathcal{T}_\tau \left\{ \hat{\psi}_s(x,\tau) \hat{\psi}_s^\dagger(0,0) \right\} \right\rangle$$

having we assumed in definition spacetime translational invariance, and being $\mathcal{T}_\tau$ the time-ordering operator. Let me take $\tau = 0^-$, thus keeping the order $\hat{\psi}\hat{\psi}^\dagger$ inside the expectation value. I (surprisingly) follow here the lead of [3, 7]: the occupation factor $n(k)$,

$$n(k) \equiv \left\langle \hat{c}_k^\dagger \hat{c}_k \right\rangle$$

is given by the Fourier transform of the equal time Green's function:

$$n(k) = \int_0^L dx\, e^{-ikx} \mathcal{G}_s(x, 0^-)$$

both for $s = \mathrm{R}, \mathrm{L}$ due to inversion symmetry. At zero temperature, the following algebraic dependence holds:

$$n(k) = n(k_F) - A \times \mathrm{sgn}(k - k_F)|k - k_F|^\zeta \qquad \zeta \equiv \frac{1}{4}\left(K + \frac{1}{K} - 2\right)$$

with $A \in \mathbb{R}$. Then, a suitable way to extract the K parameter on a lattice model simulation would be to perform the following computation:

$$n(k) \simeq \left\langle \mathrm{FT}\left\{\hat{c}_j^\dagger \hat{c}_j\right\}\right\rangle = \frac{1}{\sqrt{L}} \sum_{j=1}^{L} \left\langle \hat{c}_j^\dagger \hat{c}_j \right\rangle e^{ikj}$$

From this measure ζ can be extracted for $k < k_F$ and $k > k_F$, and from the latter K.

1.3 Bosonized correlations

This section is actually a propagation of the above section, born because correlations have particular importance in the Bosonization framework, and in understanding the different phases.

1.3.1 Equal-time density-density correlations

A very important feature of the bosonization scheme is the possibility of computing first-order analytical expressions for the correlations of observables. Take density-density correlations,

$$\mathcal{C}_{\mathrm{CDW}}(x) = \langle \delta\hat{\rho}(x)\delta\hat{\rho}(0)\rangle = \langle \hat{\rho}(x)\hat{\rho}(0)\rangle - \langle \hat{\rho}(x)\rangle \langle \hat{\rho}(0)\rangle$$

I will sketch briefly the derivation of the analytical expression for this correlation function. All details are described in [3, 5]. To treat this expression in a field-theoretical fashion, I express the density operator as

$$\begin{aligned}
\hat{\rho}(x) =: & \left[\hat{\psi}_{\mathrm{R}}^\dagger(x) + \hat{\psi}_{\mathrm{L}}^\dagger(x)\right]\left[\hat{\psi}_{\mathrm{R}}(x) + \hat{\psi}_{\mathrm{L}}(x)\right] : \\
&= -\frac{1}{\pi}\nabla\hat{\phi}(x) + \left[\hat{\psi}_{\mathrm{R}}^\dagger(x)\hat{\psi}_{\mathrm{L}}(x) + \hat{\psi}_{\mathrm{L}}^\dagger(x)\hat{\psi}_{\mathrm{R}}(x)\right] \\
&= \underbrace{-\frac{1}{\pi}\nabla\hat{\phi}(x)}_{\text{smooth}} + \underbrace{\frac{1}{2\pi\alpha}\left[e^{i2k_F x}e^{-i2\hat{\phi}(x)} + \mathrm{h.c.}\right]}_{\text{rapidly oscillating}}
\end{aligned}$$

Recall, α is a cutoff I introduced to stabilize the theory. In particular, α has the dimensions of a length and the momentum integral is cut at momenta larger than $1/\alpha$. I have split the above expression in two parts: the first is smooth, slowly oscillating on length scales k_F^{-1}. The second is rapidly oscillating. The two do not mix when computing $\mathcal{C}_{\mathrm{CDW}}(x)$, thus can be computed separately. Miranda does so [5, Sec. XIV.2], obtaining

$$\mathcal{C}_{\mathrm{CDW}}(x) \simeq \underbrace{-\frac{K}{2\pi^2 x^2}}_{\text{smooth}} + \underbrace{\frac{2}{(2\pi\alpha)^2}\cos(2k_F x)\left(\frac{\alpha}{x}\right)^{2K}}_{\text{rapidly oscillating}} \tag{14}$$

I once again indicated the smooth and rapid parts explicitly. As Giamarchi notes [3, Sec. 2.2.2], the first term reproduces a standard Fermi liquid correlation, decaying as x^{-2} with an amplitude renormalized by interactions. The second term is highly unusual and has two remarkable properties: an amplitude modulation of wavevector $2k_F$ (a property also present in Fermi liquids, signaling the presence of a Fermi sea underneath the interactions) *plus* a power-law decay whose strength is determined by interactions.

Moreover, notice that for a 1D lattice of lattice spacing a at half-filling, the Fermi wavevector is given by $k_F = \pi/2a$. Since each site coordinate is $x_r = ra$, one has

$$\mathcal{C}_{\mathrm{CDW}}(r) \simeq -\frac{K}{2\pi^2(ra)^2} + \frac{2(-1)^r}{(2\pi\alpha)^2}\left(\frac{\alpha}{ra}\right)^{2K} \quad \text{for} \quad r \in \mathbb{Z} \mod L$$

The oscillatory character of the correlation function with the site index parity reflects the fact that, at half-filling, charge-density waves (CDW) excitations have wavelength twice the lattice spacing. At unitary filling, such oscillatory behavior vanishes due to the halving of the Fermi wavevector.

1.3.2 Superconducting pairing correlations

The "superconducting" phase is gapless and governed by a tendency to fermion pairing. Consider the NN-pairing operator

$$\hat{\psi}(x)\hat{\psi}(x)$$

Of course, defined like this, such an operator identically vanishes: two fermions cannot be annihilated simultaneously at x. Consider the slight extension

$$\hat{\mathcal{O}}_{\mathrm{SU}}(x) \equiv \hat{\psi}(x+\delta x)\hat{\psi}(x)$$

For a lattice the spatial shift can be taken to be $\delta x = a$, the lattice spacing. This operator describes for a lattice the tendency to pairing *locally*. Now, when expanded in terms of Right and Left fields,

$$\begin{aligned}\hat{\psi}(x+a)\hat{\psi}(x) &= \left[\hat{\psi}_{\mathrm{R}}(x+a) + \hat{\psi}_{\mathrm{L}}(x+a)\right]\left[\hat{\psi}_{\mathrm{R}}(x) + \hat{\psi}_{\mathrm{L}}(x)\right] \\ &= (\mathrm{RR}) + (\mathrm{RL}) + (\mathrm{LR}) + (\mathrm{LL})\end{aligned}$$

the (RR) and (LL) terms are strongly suppressed in the $a \to 0$ term due to Pauli principle. The terms (RL) and (LR) are dominant. Since

$$\begin{aligned}(\mathrm{RL}) + (\mathrm{LR}) &= \hat{\psi}_{\mathrm{R}}(x+a)\hat{\psi}_{\mathrm{L}}(x) + \hat{\psi}_{\mathrm{L}}(x+a)\hat{\psi}_{\mathrm{R}}(x) \\ &= e^{ik_Fa}\hat{\Psi}_{\mathrm{R}}(x+a)\hat{\Psi}_{\mathrm{L}}(x) + e^{-ik_Fa}\hat{\Psi}_{\mathrm{L}}(x+a)\hat{\Psi}_{\mathrm{R}}(x) \\ &= e^{ik_Fa}\hat{\Psi}_{\mathrm{R}}(x+a)\hat{\Psi}_{\mathrm{L}}(x) - e^{-ik_Fa}\hat{\Psi}_{\mathrm{R}}(x)\hat{\Psi}_{\mathrm{L}}(x+a) \\ &\simeq 2i\sin(k_Fa)\hat{\Psi}_{\mathrm{R}}(x)\hat{\Psi}_{\mathrm{L}}(x) \\ &\simeq \frac{i\sin(k_Fa)}{\pi\alpha}e^{-i\left[\hat{\phi}(x)+\hat{\theta}(x)\right]}e^{i\left[\hat{\phi}(x)-\hat{\theta}(x)\right]} \\ &\simeq \frac{i\sin(k_Fa)}{\pi\alpha}e^{-2i\hat{\theta}(x)} \\ (\text{@ half filling}) &\simeq \frac{i}{\pi\alpha}e^{-2i\hat{\theta}(x)}\end{aligned}$$

I used a sequence of approximations: the continuum limit was taken, $a \to 0$, using the slow variation of the shifted fields $\hat{\Psi}_s$; then the fields $\hat{\Psi}_s$ were written explicitly in terms of their bosonic counterpart (ignoring the Klein factors), and finally I merged the two exponential operators ignoring the correction terms.

The superconducting correlator is defined as

$$\mathcal{C}_{\mathrm{SU}}(x) = \left\langle \hat{\mathcal{O}}^\dagger_{\mathrm{SU}}(x)\hat{\mathcal{O}}_{\mathrm{SU}}(0)\right\rangle$$

It can be shown that previous result give:

$$\mathcal{C}_{\mathrm{SU}}(x) = \frac{1}{(\pi\alpha)^2}\left(\frac{\alpha}{x}\right)^{2/K} \tag{15}$$

The most important detail to notice with respect to the CDW correlator of Eq. (14) is the inverted power-law dependence. This feature ensures that CDW and SU correlators are somewhat "dual" with respect to the Luttinger parameter K: as K gets bigger than 1, superconducting correlations are boosted while charge correlations are suppressed. The situation is inverted as $K < 1$ gets smaller. A schematics of this behavior is given in Fig. 4.

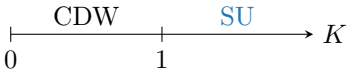

Figure 4 | Schematic illustration of the dominant correlator (charge density wave or superconducting) for different values of $K \geq 0$. The CDW phase is confined by $0 \leq K \leq 1$, while the SU phase is given by $K \geq 1$.

1.3.3 Meaning of the Luttinger parameter K

The Luttinger parameter K ultimately contains all the relevant physics of the problem. As Giamarchi explains [3, Sec. 2.2.2], correlations are connected to imaginary-time (and dynamical) susceptibilities. The very key point is that a power-law scaling of correlations translates in an analogous power-law scaling of susceptibilities, which leads to integer-order poles in these last. This passage is made by Fourier-transforming quantities in three dimensions, and considering the low-dimensionality as a constraint.

It turns out, $K = 1$ discriminates two "regions". For $K < 1$, SU correlations are strongly suppressed and so is the respective susceptibility. The state does not respond to superconducting pairing. Inversely, CDW correlations and susceptibility diverge. The state tends to order accordingly. Particles do not pair: interactions are repulsive. The situation is flipped for $K > 1$, with the divergent correlation now being the superconducting one. The dominant interaction is now attractive.

This is a matter of identifying the most divergent fluctuation in one dimension, which is, the most likely to be stabilized by an arbitrarily weak three-dimensional coupling [3]. This is most true for extreme Luttinger parameter values, $K \to 0$ or $K \gg 1$. This confused comment ends this section: in the next, I study theoretically and bosonize a spinless Fermi-Hubbard chain.

2 The Fermi-Hubbard model

In this project I limit myself to a polarized (spinless fermions) system. Extension to a spinful system is possible and introduces some refinements in the general bosonization scheme, the most notable being the famous spin-charge separation. Let me take it easy: consider the following interacting hamiltonian:

$$\hat{H} \equiv -t \sum_{\langle j,k \rangle} \left[\hat{c}_j^\dagger \hat{c}_k + \hat{c}_k^\dagger \hat{c}_j \right] + V \sum_{\langle j,k \rangle} \hat{n}_j \hat{n}_k - \mu \sum_{j=1}^{L} \hat{n}_j \tag{16}$$

defined on a closed one-dimensional lattice ring, as in Fig. 5a. This is a simple nearest-neighbors (NN) interacting lattice hamiltonian with NN interaction V, chemical potential μ and hopping amplitude t,

$$t, V, \mu \in \mathbb{R}$$

I will also be considering a magnetic flux Φ threading the ring and coupling to the charge degree of freedom. On a ring this pinned flux acts as a tangential vector potential, which is, a momentum offset; thus the correct way to absorb into our lattice framework this interaction is via the pseudo-gauge transformation

$$\hat{c}_j \to e^{-ij\phi} \hat{c}_j \qquad \hat{c}_j^\dagger \to e^{ij\phi} \hat{c}_j^\dagger \qquad \phi \equiv \frac{\Phi}{L} \tag{17}$$

Incorporate the latter in the above hamiltonian: the hopping amplitude becomes complex (which is, chiral) $t \to T \equiv te^{i\phi}$, with $t, \phi \in \mathbb{R}$. We have, as in Fig. 5b

$$\hat{H} \equiv -t \sum_{j=1}^{L} \left[e^{-i\phi} \hat{c}_j^\dagger \hat{c}_{j+1} + e^{i\phi} \hat{c}_{j+1}^\dagger \hat{c}_j \right] + V \sum_{j=1}^{L} \hat{n}_j \hat{n}_{j+1} - \mu \sum_{j=1}^{L} \hat{n}_j \tag{18}$$

where a $\mod L$ operation is intended: $L+1 \leftrightarrow 1$. I want to indagate its ground-state properties. The relevant parameters will be the reduced interaction V/t and chemical potential μ/t.

$V/t > 0$	Repulsive interaction
$V/t < 0$	Attractive interaction

Intuitively, if the interaction becomes dominant with respect to the hopping dynamics, the combined effect of attraction/repulsion and Pauli exclusion principle should lead to two different forms of localization. On one hand, if the interaction is strong and attractive, the ground state should be uniformly filled, because fermions save energy both by closely packing and by increasing density due to the negative chemical potential contribution ($\mu > 0$). On the other hand, a strong repulsive interaction could lead to an half-filled chain, which sacrifices the chemical potential energy gain lost by reducing the particle number by not paying the energy cost of having nearby fermions. In both cases hopping is suppressed, thus fermions are localized; now it is a matter of seeing if these states are actually realized.

2.1 Jordan-Wigner mapping of the Heisenberg XXZ model

The model presented above can be obtained rather easily through a Jordan-Wigner of the Heisenberg XXZ model in transverse field,

$$\hat{H}_{\text{XXZ}} \equiv \sum_{\langle j,k \rangle} \left[J_{xy} \left(\hat{S}_j^x \hat{S}_k^x + \hat{S}_j^y \hat{S}_k^y \right) + J_z \hat{S}_j^z \hat{S}_k^z \right] - h \sum_{j=1}^{L} \hat{S}_j^z \tag{19}$$

The Jordan-Wigner mapping, only feasible in one dimension due to sites ordering, is given by:

$$\hat{S}_j^+ \to \hat{c}_j^\dagger e^{i\pi \sum_{k<j} \hat{c}_k^\dagger \hat{c}_k} \qquad \hat{S}_j^- \to \hat{c}_j e^{-i\pi \sum_{k<j} \hat{c}_k^\dagger \hat{c}_k} \qquad \hat{S}_j^z \to \hat{n}_j - \frac{\mathbb{I}}{2}$$

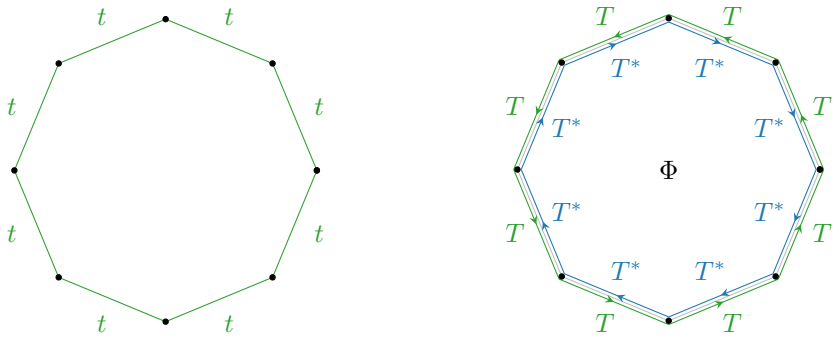

a | Lattice with null flux. b | Lattice with finite flux Φ.

Figure 5 | In Fig. 5a a schematics of a $1D$ closed lattice is portrayed. The hopping amplitude t is purely real, $t = \mathrm{sgn}(t)|t|$. In Fig. 5b the same lattice is represented, but coupled to a finite threading flux Φ which can be absorbed via the pseudo-gauge transformation in Eq. (17). As a consequence, the hopping amplitude acquires a chirality which manifests in a non-null imaginary part, $T = te^{i\Phi/L}$.

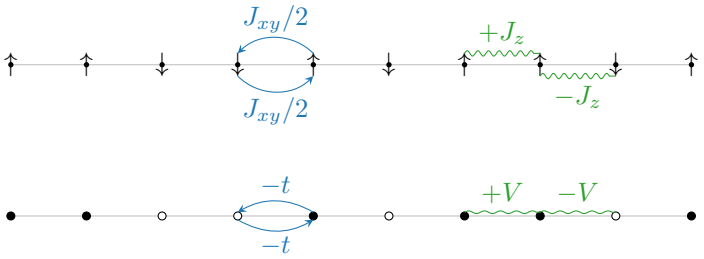

Figure 6 | Schematics of the Jordan-Wigner mapping. The above chain represents the XXZ model, while the chain below represents the spinless Fermi-Hubbard model. Hollow circles represent holes, filled circles represents on-site particles. In both chain the two competing processes are represented: the NN interaction and the swapping interaction.

It can be shown rather easily that, if the c-operators are canonically fermionic (which is, $\{c_j, c_k^\dagger\} = \delta_{jk}$) then the 3D $\mathfrak{su}(2)$ spin algebra is preserved by this mapping. Notice the appearance of the Jordan parity operator up to site $j-1$, $\hat{\mathrm{P}}_{j-1}$, with

$$\hat{\mathrm{P}}_\ell = e^{i\pi \sum_{k\leq \ell} \hat{c}_k^\dagger \hat{c}_k} \quad \to \quad (-1)^{\zeta_\ell} \qquad \zeta_\ell \equiv \sum_{k\leq \ell} \hat{n}_k$$

Essentially, the above string counts the fermions *before* the site in question and gives back a factor $+1$ for even number, -1 for odd number. This works for open-ends chains, where the concept of *before* is actually well-defined.

Using basic algebra, it is straightforward to see:

$$S_j^+ \hat{S}_{j+1}^- \to \left(\hat{\mathrm{P}}_{j-1}\hat{c}_j^\dagger\right)\left(\hat{\mathrm{P}}_j \hat{c}_{j+1}\right) = \hat{c}_j^\dagger \hat{c}_{j+1}$$
$$S_j^- \hat{S}_{j+1}^+ \to \left(\hat{\mathrm{P}}_{j-1}\hat{c}_j\right)\left(\hat{\mathrm{P}}_j \hat{c}_{j+1}^\dagger\right) = \hat{c}_{j+1}^\dagger \hat{c}_j$$

Indeed, the product operator $c_j^\dagger \hat{\mathrm{P}}_j$ vanishes if the site j is occupied. Then site j does not contribute to parity, giving $\mathrm{P}_{j-1} = \mathrm{P}_j$. Identical reasoning holds for the line below, completed by an anticommutation of Fermi operators. Let me take a 1D spin chain with open boundary conditions

(OBC). The transformation gives

$$\begin{aligned}\hat{H}_{\mathrm{XXZ}} &\equiv \sum_{j=1}^{L-1}\left[\frac{J_{xy}}{2}\left(\hat{S}_j^+\hat{S}_{j+1}^- + \hat{S}_j^-\hat{S}_{j+1}^+\right) + J_z\hat{S}_j^z\hat{S}_{j+1}^z\right] - h\sum_{j=1}^{L}\hat{S}_j^z \\ &= \sum_{j=1}^{L-1}\left[\frac{J_{xy}}{2}\left(\hat{c}_j^\dagger\hat{c}_{j+1} + \hat{c}_{j+1}^\dagger\hat{c}_j\right) + J_z\left(\hat{n}_j - \frac{\mathbb{I}}{2}\right)\left(\hat{n}_{j+1} - \frac{\mathbb{I}}{2}\right)\right] - h\sum_{j=1}^{L}\left(\hat{n}_j - \frac{\mathbb{I}}{2}\right) \\ &= \sum_{j=1}^{L-1}\left[\frac{J_{xy}}{2}\left(\hat{c}_j^\dagger\hat{c}_{j+1} + \hat{c}_{j+1}^\dagger\hat{c}_j\right) + J_z\hat{n}_j\hat{n}_{j+1}\right] - \sum_{j=1}^{L}h_j\hat{n}_j + \frac{hL}{2} + \frac{J_z(L-1)}{2}\end{aligned}$$

where I defined:

$$h_j = \begin{cases} h + J_z/2 & \text{if} \quad j = 1, L \\ h + J_z & \text{if} \quad 1 < j < L \end{cases}$$

Notice that for OBC the field term at the ends of the chain misses half the J_z correction to the field, because of the missing interaction link.

Now I close the chain. This amounts to add a new interaction term,

$$\hat{H}_{\mathrm{XXZ}} \to \hat{H}_{\mathrm{XXZ}} + \frac{J_{xy}}{2}\left(\hat{S}_L^+\hat{S}_1^- + \hat{S}_L^-\hat{S}_1^+\right) + J_z\hat{S}_L^z\hat{S}_1^z$$

Jordan-Wigner mapping requires a little more care here. Since

$$\begin{aligned}\hat{S}_L^+\hat{S}_1^- &= \left(\hat{\mathrm{P}}_{L-1}\hat{c}_L^\dagger\right)\hat{c}_1 = \left(\hat{\mathrm{P}}_L\hat{c}_L^\dagger\right)\hat{c}_1 = (-1)^{\#_F-1}c_L^\dagger\hat{c}_1 \\ \hat{S}_L^-\hat{S}_1^+ &= \left(\hat{\mathrm{P}}_{L-1}\hat{c}_L\right)\hat{c}_1^\dagger = \left(-\hat{\mathrm{P}}_L\hat{c}_L\right)\hat{c}_1^\dagger = -(-1)^{\#_F+1}c_L\hat{c}_1^\dagger = (-1)^{\#_F+1}\hat{c}_1^\dagger c_L\end{aligned}$$

The first line holds because the L-th site must be empty, thus leaving unchanged the parity operator when extending $\mathrm{P}_{L-1} \to \mathrm{P}_L$, and simultaneously to evaluate the total chain parity after having applied $\hat{c}_1$ gives non-zero result only if the first site is occupied. Then, calling $\#_F$ the total number of fermions on the chain, the final parity is $\# - 1$ which accounts for the first line sign prefactor. An analogous argument holds as well for the second line. We conclude that:

- if the total number of fermions on the chain is **odd**, $\#_F = 2n+1$ for $n \in \mathbb{N}$, we can add the new interaction term to the hamiltonian with identical form,

$$\hat{H}_{\mathrm{XXZ}} = \sum_{j=1}^{L}\left[\frac{J_{xy}}{2}\left(\hat{c}_j^\dagger\hat{c}_{j+1} + \hat{c}_{j+1}^\dagger\hat{c}_j\right) + J_z\hat{n}_j\hat{n}_{j+1}\right] - (h + J_z)\sum_{j=1}^{L}\hat{n}_j \qquad (\hat{c}_{L+1} \equiv \hat{c}_1) \quad (20)$$

  I neglected an irrelevant energy shift. The PBC-XXZ model is mapped onto a spinless fermion system with odd number of fermions.

- if the total number of fermions on the chain is **even**, $\#_F = 2n+1$ for $n \in \mathbb{N}$, we can add the new interaction term to the hamiltonian closing the chain anti-periodically (or, equivalently, flipping the sign of the nearest-neighbor hopping term across the closing link),

$$\hat{H}_{\mathrm{XXZ}} = \sum_{j=1}^{L}\left[\frac{J_{xy}}{2}\left(\hat{c}_j^\dagger\hat{c}_{j+1} + \hat{c}_{j+1}^\dagger\hat{c}_j\right) + J_z\hat{n}_j\hat{n}_{j+1}\right] - (h + J_z)\sum_{j=1}^{L}\hat{n}_j \quad (\hat{c}_{L+1} \equiv -\hat{c}_1)$$

  The APBC-XXZ model is mapped onto a spinless fermion system with even[4] number of fermions.

[4]This is a matter of exact mappings. However it is intuitively clear that for large enough chains, a single inverted bond has null impact on the general phase structure of the model – just as borders normally to for OBC systems. In thermodynamic limit, one expects the fermion parity to be irrelevant in terms of models mapping coherence.

Figure 7 | Schematics for the XXZ model phase diagram. We are here considering a zero-field model, $h = 0$ (which is mapped by the maps (21) to a $\mu = J_z$ model). H indicates Heisenberg, I indicates Ising; F stands for Ferromagnet, AF for Anti-Ferromagnet; XY stands for pure XY model. The color of each label recalls the dominant interaction of Fig. 6.

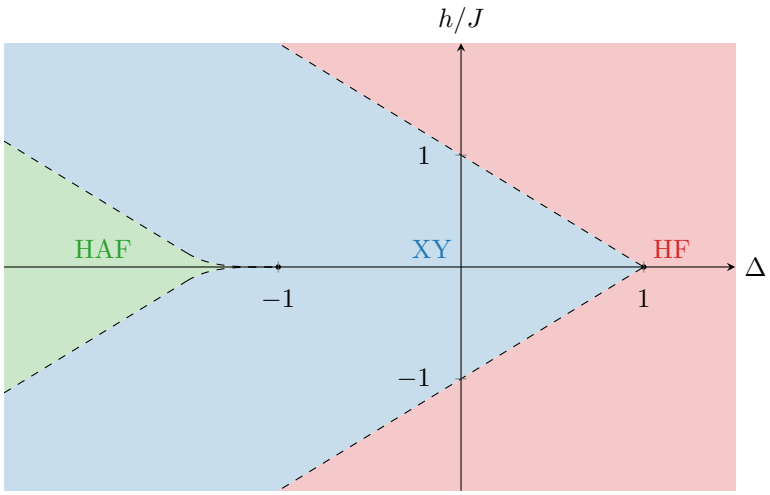

Figure 8 | Schematics of the phase boundaries for the XXZ model as extracted by Franchini [2, Sec. 4.1]. Notice the two zero-field phase-transition points $(-1, 0)$ and $(1, 0)$.

For the sake of simplicity, I will limit this project to the first situation with an odd number of fermions. Since the PBC-XXZ admits for an exact Bethe-Ansatz solution, we can link the phase transitions of the two models. Apart from a constant energy shift, the hamiltonian (20) is *de-facto* identical to the spinless model of Eq. (16) via the mapping

$$t = -\frac{J_{xy}}{2} \qquad V = J_z \qquad \mu = h + J_z \tag{21}$$

A schematics of this mapping is given in Fig. 6.

Phase diagrams

The phase diagram of the XXZ model is readily obtained by the means of exact methods like Bethe Ansatz. Of course, the dominant parameter is the ratio J_z/J_{xy} which measures the dominant contribution to energy given by spin-spin NN interaction (z term) and spin diffusion (xy term). Whenever $|J_z| = |J_{xy}|$, the model is of the Heisenberg class. We can safely assume $J_{xy} < 0$ and only consider the relative sign of J_z. This is easily seen: if we map

$$J_{xy} \to -J_{xy} \qquad J_z \to J_z$$

which is, exchange the hopping sign, this is equivalent to flipping the sign of the xy spin component while leaving the z component unchanged. Such a map is canonical (does not impact the spin algebra). The phase diagram for negative-sign hopping is anti-symmetric with respect to this inversion. The same holds for finite field. The basic, field free phase diagram is represented schematically in Fig. 7.

1. The system tends to an Ising Anti-Ferromagnet for $J_z/J_{xy} < -1$, with dominant behavior the complete anti-alignment of spins (which maps onto the spinless Fermi-Hubbard model as an half-filled chain).

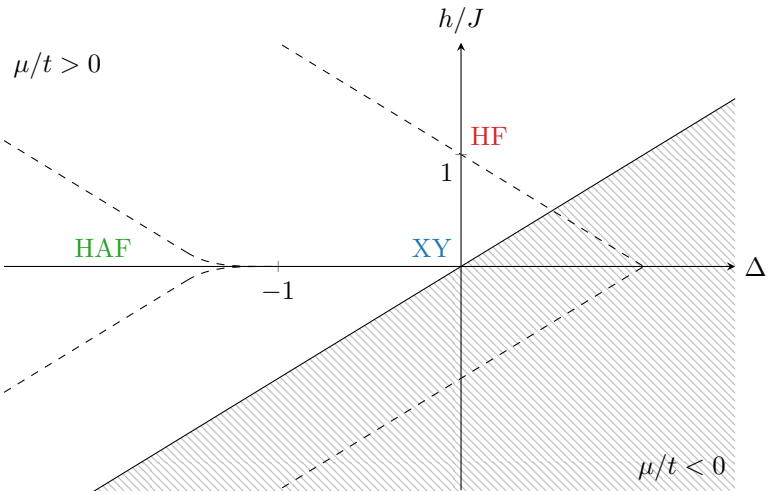

Figure 9 | The same phase diagram as in Fig. 8, completed with the requirement $h/J < \Delta$. The shaded area is excluded from the mapping. Note that a positive chemical potential excludes the Antiferromagnetic phase.

2. Moving across the first Heisenberg boundary, $J_z = -J_{xy}$, the dominant behavior for energy lowering is spin diffusion up to a perfect local fields free situation of $J_z = 0$. This phase maps onto the spinless Fermi-Hubbard model as a superconducting phase.

3. Crossing the second Heisenberg boundary, $J_z = J_{xy}$, the system tends to an Ising Ferromagnet, dominated by the uniform state configuration. The latter maps onto a completely filled fermionic chain.

For a fixed number system, this is the expected phase dynamics, schematically represented in Fig. 7. Now, define J and Δ as does Franchini in [2, Sec. 4.1], which is

$$J_{xy} \equiv -J \qquad J_z \equiv -J\Delta$$

This gives the mapping:

$$t = \frac{J}{2} \qquad \frac{V}{t} = -2\Delta \qquad \frac{\mu}{t} = 2\left(\frac{h}{J} - \Delta\right) \tag{22}$$

Within this parametrization, the analytical phase diagram[5] is the one depicted in Fig. 8. Now, I use $\mu/t > 0$. This maps on the XXZ model as $h/J > \Delta$, a condition depicted in Fig. 9. Expressing the phase borders as functions of Δ, one is able to map the phase diagram of the PBC-XXZ model onto the spinless Fermi-Hubbard phase diagram of Fig. 10. Three phases are present, as expected intuitively. Two are Mott-localized, respectively with unitary filling (MI_1 in figure) and with half-filling ($\mathrm{MI}_{1/2}$ in figure).

Such a phase diagram is easy to explain physically. Three mechanisms are present: the NN interaction repels or attracts fermions, the hopping part favors density diffusion, the chemical potential gains favor by incrementing the total density. If the interaction is strongly attractive, energy is lowered by maximizing the number of fermions – we are in the MI_1 phase on the left. If the interaction is strongly repulsive, either the system gains energy by keeping the density low and delocalized (energy is gained thanks to the spatial superposition of the wavefunction across sites) or, if the chemical potential is large enough, by maximizing the particles number while minimizing the number of pairs across nearest neighbors sites – we are in the $\mathrm{MI}_{1/2}$ phase on the left. In between, the expected phase is expected to present superconducting (SU) features. Running simulations in a regime $\mu/t > 0$ and $V/t \in \mathbb{R}$, what one expects is to encounter all three phases. Now, I need to reconnect this expectation in a bosonization framework.

[5] This phase diagram is obtained exactly by the means of Bethe Ansatz [2, 6].

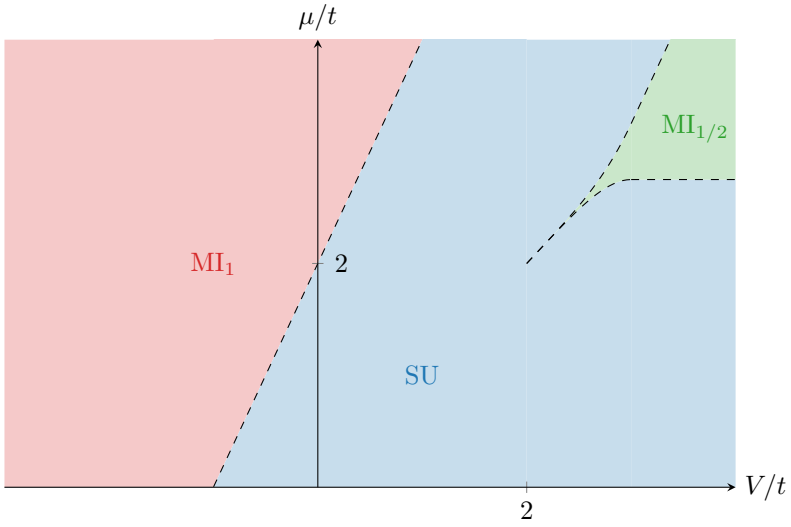

Figure 10 | The expected phase diagram for the spinless Fermi-Hubbard model, obtained thanks via the (22) mapping of the phase diagram in Fig. 8.

2.2 Non-interacting ground-state

In order to further explore the interacting system, we need to know its zero-field non-interacting ground-state. This amounts to setting $V = \mu = 0$. The hamiltonian is well known,

$$\hat{H}_0 = -t \sum_{j=1}^{L} \left(\hat{c}_j^\dagger \hat{c}_{j+1} + \hat{c}_{j+1}^\dagger \hat{c}_j \right)$$

and is easily solved by a simple Fourier transformation,

$$\hat{c}_j \equiv \sum_k e^{ikj} \hat{c}_k$$

(I am here using adimensional momenta k, since space has throughout been considered as a simple integer index) which leads to

$$\hat{H}_0 = -t \sum_k \left[e^{-ik} \hat{c}_k^\dagger \hat{c}_k + e^{ik} \hat{c}_k^\dagger \hat{c}_k \right] = \sum_k \epsilon_k \hat{c}_k^\dagger \hat{c}_k \quad \text{for} \quad \epsilon_k = -2t \cos k \tag{23}$$

The band ϵ_k is represented in Fig. 11. At half-filling, this simple sinusoidal band presents a null Fermi energy at Fermi wavevector $k_F = \pm\pi/2$. Linearization of the band for subsequent bosonization is as well represented in Fig. 11.

2.3 Bosonization of the free model

I now *bosonize* the spinless Fermi-Hubbard model. Recall the processes of Fig. 2: for a spinless system the only contributions to a bosonized hamiltonian is from the g_2 and g_4 processes. The non-interacting hamiltonian is very simple, and it already known how to reduce it to the form of Eq. (7): all is needed is to take a coherent continuum limit for the fermionic operators,

$$\hat{c}_j \to \hat{\psi}(x)$$

Let me reintroduce a lattice spacing a for the sake of dimensional correctness. The bosonization of an hamiltonian of the kind of Eq. (23) has been treated at the very beginning of the present report. The only step to be done is the linearization depicted in Fig. 11,

$$-2t \cos(ka)\big|_{k=\pm\frac{\pi}{2a}+q} = 2t \cos\left(\pm\frac{\pi}{2} + qa\right) \simeq \pm(aJ)q$$

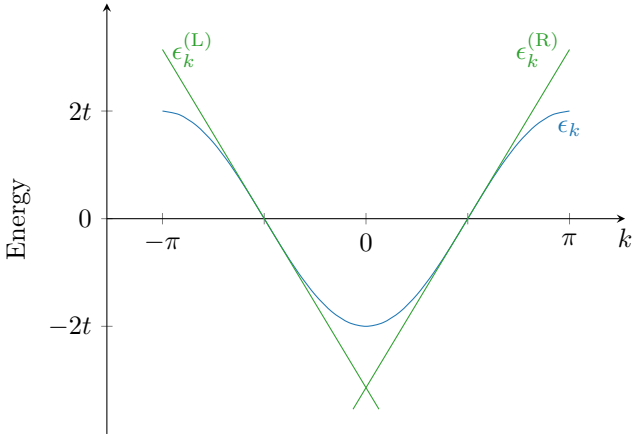

Figure 11 | Excitations band and relative linearizations for the non-interacting model ($V = 0$). At half-filling the ground-state has null Fermi energy, the negative part of the band is filled and the spectrum is gapless.

I take as granted the result of Eq. (7), recognizing the Fermi velocity simply as

$$v_F = \partial_k \epsilon_k \big|_{k=k_F} = aJ$$

(As always, I omit a term $\hbar = 1$). For the sake of completeness, here I also derive the Dirac expression for the hamiltonian density of these linear dispersion fermions (which, of course, are massless). First, split the hamiltonian of Eq. (23),

$$\hat{H}_0 \simeq \hat{H}_0^{(\mathrm{R})} + \hat{H}_0^{(\mathrm{L})} \quad \text{with} \quad \hat{H}_0^{(s)} \equiv \mathrm{sgn}(s) v_F \sum_q q \left[\hat{c}_k^{(s)}\right]^\dagger \hat{c}_k^{(s)}$$

I take a continuum limit: with fixed L, I employ $a \to 0^+$. Then, transforming back to space,

$$\hat{c}_k^{(s)} = \frac{1}{\sqrt{L}} \int_0^L dx\, e^{-ikx} \hat{\psi}_s(x)$$

Recall the shifted fields $\hat{\Psi}_s(x)$ of Eq. (3). Being q defined with respect to the Fermi point $k = \mathrm{sgn}(s)k_F$, such that $q = k - \mathrm{sgn}(s)k_F$,

$$\hat{c}_k^{(s)} = \frac{1}{\sqrt{L}} \int_0^L dx\, e^{-iqx} \hat{\Psi}_s(x)$$

Then

$$H_0^{(s)} = \mathrm{sgn}(s) \frac{v_F}{L} \sum_q q \int_0^L dx\, e^{iqx} \hat{\Psi}_s^\dagger(x) \int_0^L dy\, e^{-iqy} \hat{\Psi}_s(y)$$

Since

$$\partial_y \left[e^{-iqy} \hat{\Psi}_s(y)\right] = -iq e^{-iqy} \hat{\Psi}_s(y) + e^{-iqy} \partial_x \hat{\Psi}_s(y)$$

and integrating the left-hand side one gets zero, being the chain closed with PBC,

$$H_0^{(s)} = -i\mathrm{sgn}(s) \frac{v_F}{L} \int_0^L dx\, \hat{\Psi}_s^\dagger(x) \int_0^L dy\, \partial_x \hat{\Psi}_s(y) \sum_q e^{iq(x-y)}$$

Using the continuum limit

$$\frac{1}{L} \sum_q \quad \to \quad \frac{1}{2\pi} \int_{\mathbb{R}} dq$$

the s-side hamiltonian finally reduces to

$$H_0^{(s)} = -i\mathrm{sgn}(s)\frac{v_F}{2\pi}\int_0^L dx\, \hat{\Psi}_s^\dagger(x)\partial_x\hat{\Psi}_s(x)$$

Then the massless chiral Dirac hamiltonian is recovered:

$$\hat{H}_0 = \frac{v_F}{2\pi i}\int_0^L dx\, \left[\hat{\Psi}_{\mathrm{R}}^\dagger(x)\partial_x\hat{\Psi}_{\mathrm{R}}(x) - \hat{\Psi}_{\mathrm{L}}^\dagger(x)\partial_x\hat{\Psi}_{\mathrm{L}}(x)\right] \tag{24}$$

Now, all is left to do is to insert interactions in the bosonized hamiltonian and link the model parameters to the Luttinger parameters u and K.

2.4 Bosonization of nearest-neighbors interaction

The interaction term is of the density-density class,

$$\hat{V} = V\sum_{j=1}^{L}\hat{n}_j\hat{n}_{j+1} = a^2 J\Delta\sum_{j=1}^{L}\frac{\hat{n}_j}{a}\frac{\hat{n}_{j+1}}{a}$$

We identify $\hat{n}_j/a \to \hat{\rho}(x = ja)$ as the continuum density, thus giving (splitting in left/right contributions)

$$\hat{V} = a^2 J\Delta\sum_{j=1}^{L}\hat{\rho}(ja)\hat{\rho}\left((j+1)a\right) \tag{25}$$

The detailed derivation can be found in [3, Sec. 6.1.2]. The starting point is the expansion of $\hat{\rho}$, carried out in terms of physical fields $\hat{\psi}_s$ or shifted fields $\hat{\Psi}_s$ as defined in Eq. (3),

$$\begin{aligned}\hat{\rho}(x) &= -\frac{1}{\pi}\nabla\hat{\phi}(x) + \left[\hat{\psi}_{\mathrm{R}}^\dagger(x)\hat{\psi}_{\mathrm{L}}(x) + \hat{\psi}_{\mathrm{L}}^\dagger(x)\hat{\psi}_{\mathrm{R}}(x)\right] \\ &= -\frac{1}{\pi}\nabla\hat{\phi}(x) + \left[e^{-2ik_F x}\hat{\Psi}_{\mathrm{R}}^\dagger(x)\hat{\Psi}_{\mathrm{L}}(x) + e^{2ik_F x}\hat{\Psi}_{\mathrm{L}}^\dagger(x)\hat{\Psi}_{\mathrm{R}}(x)\right]\end{aligned} \tag{26}$$

In thermodynamic limit, recalling Eq. (6),

$$\hat{\Psi}_s(x) = \frac{\hat{U}_s}{\sqrt{2\pi\alpha}}\exp\left\{i\left(\mathrm{sgn}(s)\hat{\phi}(x) + \hat{\theta}(x)\right)\right\} \qquad (\alpha \to 0)$$

The analytical calculation gets a little cumbersome: I only highlight the essential passage. First, express analytically the density operator of Eqns. (26) using the results

$$\hat{\Psi}_{\mathrm{R}}^\dagger(x)\hat{\Psi}_{\mathrm{L}}(x) = \frac{\hat{U}_{\mathrm{R}}^\dagger\hat{U}_{\mathrm{L}}}{2\pi\alpha}e^{-2i\hat{\phi}(x)} \qquad \hat{\Psi}_{\mathrm{L}}^\dagger(x)\hat{\Psi}_{\mathrm{R}}(x) = \frac{\hat{U}_{\mathrm{L}}^\dagger\hat{U}_{\mathrm{R}}}{2\pi\alpha}e^{2i\hat{\phi}(x)}$$

which gives

$$\hat{\rho}(x) = -\frac{1}{\pi}\nabla\hat{\phi}(x) + \left[e^{-2ik_F x}\frac{\hat{U}_{\mathrm{R}}^\dagger\hat{U}_{\mathrm{L}}}{2\pi\alpha}e^{-2i\hat{\phi}(x)} + e^{2ik_F x}\frac{\hat{U}_{\mathrm{L}}^\dagger\hat{U}_{\mathrm{R}}}{2\pi\alpha}e^{2i\hat{\phi}(x)}\right] \tag{27}$$

Insert now the above result in Eq. (25) for both the densities appearing. The key property to be used here is that the shifted fields $\hat{\Psi}_s$ (and hence the bosonic fields) vary *slowly* with respect to k_F. This means that, in the limit $a \to 0$ of null lattice spacing, one can approximate the spatial variation as only happening in the fast-oscillating exponents of the above equation. This assumption limits this derivation to slight fluctuations of the fields around equilibrium, which means, to perturbative results. Moreover, one identifies the cutoff α with a, sending both to zero. The two densities multiplied in Eq. (25) then give rise to $3 \times 3 = 9$ terms, of which the most relevant are

- the one coming from the ϕ field gradients multiplied,

$$\frac{1}{\pi^2}\nabla\hat{\phi}(x)\nabla\hat{\phi}(x+a) \simeq \frac{1}{\pi^2}\left(\nabla\hat{\phi}(x)\right)^2$$

  Such approximation is possible because, as said, fields vary slowly and then $x+a$ can be taken to be x as well when a field variable;

- the one coming from the multiplication of the second term of Eq. (27) (evaluated at x) with the third one (evaluated at $x+a$)

$$e^{-2ik_F x}\frac{\hat{U}_{\mathrm{R}}^\dagger\hat{U}_{\mathrm{L}}}{2\pi a}e^{-2i\hat{\phi}(x)} \times e^{2ik_F(x+a)}\frac{\hat{U}_{\mathrm{L}}^\dagger\hat{U}_{\mathrm{R}}}{2\pi a}e^{2i\hat{\phi}(x+a)} = \frac{1}{(2\pi a)^2}e^{2ik_F a}e^{2i\left[\hat{\phi}(x+a)-\hat{\phi}(x)\right]}$$

  where I dropped the Klein factors and substituted $\alpha \to a$;

- the hermitian conjugate of the above term, which arises inverting the roles in the previous point.

The other terms either vanish when summed to their respective hermitian conjugate or are subdominant[6]. Then

$$\hat{\rho}(x)\hat{\rho}(x+a) \simeq \frac{1}{\pi^2}\left(\nabla\hat{\phi}(x)\right)^2 + \frac{1}{(2\pi a)^2}e^{2ik_F a}e^{2i\left[\hat{\phi}(x+a)-\hat{\phi}(x)\right]} + \frac{1}{(2\pi a)^2}e^{-2ik_F a}e^{-2i\left[\hat{\phi}(x+a)-\hat{\phi}(x)\right]}$$

Finally, approximating

$$\begin{aligned} e^{\pm 2i\left[\hat{\phi}(x+a)-\hat{\phi}(x)\right]} &\simeq e^{\pm 2ia\nabla\hat{\phi}(x)} \\ &\simeq 1 \pm 2ia\nabla\hat{\phi}(x) - 2a^2\left(\nabla\hat{\phi}(x)\right)^2 \end{aligned}$$

The 1 constant term can be discarded: it only generates a constant energy shift. The linear terms $\pm 2ia\nabla\hat{\phi}(x)$ can be discarded as well, since they vanish when summed. Only the last survives:

$$\begin{aligned} \hat{\rho}(x)\hat{\rho}(x+a) &\simeq \frac{1}{\pi^2}\left(\nabla\hat{\phi}(x)\right)^2 - \frac{2a^2}{(2\pi a)^2}\left(\nabla\hat{\phi}(x)\right)^2\left(e^{2ik_F a}+e^{-2ik_F a}\right) \\ &= \frac{1}{\pi^2}\left(\nabla\hat{\phi}(x)\right)^2\left(1-\cos(2k_F a)\right) \\ \text{(at half filling)} &= \frac{2}{\pi^2}\left(\nabla\hat{\phi}(x)\right)^2 \end{aligned}$$

It's done. Recalling the bosonic structure of the general bosonized spinless Luttinger hamiltoninan of Eq. (9), we finally conclude that the bosonized interacting hamiltonian is given by

$$\frac{1}{2\pi}\int_0^L dx\left[\frac{u}{K}\left(\nabla\hat{\phi}(x)\right)^2 + uK\left(\nabla\hat{\theta}(x)\right)^2\right] \quad \text{with} \quad \begin{cases} uK &= aJ \\ u/K &= aJ\left(1+4\Delta/\pi\right) \end{cases} \tag{28}$$

This simple result is a consequence of the many approximations I made. It is far from exact and strictly perturbative. By the means of Bethe Ansatz, a much better result can be obtained. It must be said, by the time the author got to this point, the hopes for the simulated data to be anywhere near any of these results were narrow.

[6] A word of caution fits here. Another term actually appears in the expansion, namely a *umklapp* term. As is explained by Giamarchi in [3, Sec. 6.1.2], for a spinless hamiltonian defined on a lattice this term is less relevant when compared to the others (but is far from irrelevancy for a complete physical description!).

3 Algorithms and simulations

This section is devoted to delineate the system properties we aim to simulate. The algorithm used is finite-size DMRG, implemented in the Julia language via the well supported ITensors.jl, ITensorsMPS.jl packages. The hamiltonian of Eq. (16) was simply implemented,

```
function GetHamiltonianMPO(
        sites::Any,      # Sites
        t::Float64,      # Hopping
        V::Float64,      # Interaction
        mu::Float64;     # Chemical pontential
        Phi=0            # Flux
    )::MPO

    os = OpSum()
    L = length(sites)

    for j=1:L

        # Separate:  initialize Float64 or ComplexFloat64
        if Phi!==0
            os += -t * (cos(Phi/L) - im*sin(Phi/L)),"Cdag",j,"C",
                mod1(j+1,L)
            os += -t * (cos(Phi/L) + im*sin(Phi/L)),"Cdag",mod1(j
                +1,L),"C",j
        elseif Phi==0
            os += -t,"Cdag",j,"C",mod1(j+1,L)
            os += -t,"Cdag",mod1(j+1,L),"C",j
        end

        os += V,"N",j,"N",mod1(j+1,L)
        os += -mu,"N",j

    end

    return MPO(os, sites)
end
```

I inserted the above snippet to give a feel of the easiness of the packages in Julia language. Finite-size DMRG method is a built-in method in the packages. The entirety of the code, as said, is openly accessible at this repository.

3.1 What I would have liked to do (better)

A good target is to extract the Bosonization parameters u and K for the spinless Fermi-Hubbard model of Eq. (16). As said in Sec. 1.2, for a spinless model the task can be easy enough by performing the calculation of the charge compressibility κ and the charge stiffness $\mathcal{D}$. From Eq. (11) and (13) respectively,

$$\kappa = \frac{K}{\pi u} \qquad \text{and} \qquad \mathcal{D} = uK \tag{29}$$

which in turn implies

$$u = \sqrt{\frac{\mathcal{D}}{\pi\kappa}} \qquad \text{and} \qquad K = \sqrt{\pi\kappa\mathcal{D}} \tag{30}$$

Coherently with the definitions I used, the observables κ and $\mathcal{D}$ were calculated as follows. Let me define:

$$E_g\left[L, N, \eta; \frac{V}{t}, \frac{\mu}{t}\right] \tag{31}$$

as the ground-state energy for the model setup specified by its arguments L (size), N (number of particles), η (adimensional magnetic flux) and parameters V/t (reduced NN interaction) and μ/t (reduced chemical potential). From now on I omit V/t and μ/t as explicit parameters.

Charge compressibility. Charge compressibility is given by

$$\kappa^{-1} = L\frac{\partial^2 E}{\partial N^2}$$

which is well approximated at half-filling by

$$\kappa_{1/2}(L) \equiv \left[\frac{E_g[L, L/2+2, 0] + E_g[L, L/2-2, 0] - 2E_g[L, L/2, 0]}{4}\right]^{-1} \tag{32}$$

(usually one adds or removes 2 particles in order to avoid even-odd effects). This strategy is good for mapping the compressibility in the canonical ensemble, for which the energy is minimized each time given a fixed particles number. For a mapping of compressibility over the $[V/t, \mu/t]$ evidently one needs to let the particles number vary in order to find the gran-canonical ground state. I adopted a rather rough but coherent strategy, approximated the compressibility via its finite-differences derivative formulation

$$\kappa \simeq \frac{\Delta\rho}{\Delta\mu} = \frac{1}{L}\frac{\Delta}{\Delta\mu}\langle\hat{N}\rangle$$

where $\langle\hat{N}\rangle$ is the expected total particles number evaluated at two subsequent simulations with identical V/t and chemical potential differing by $\Delta\mu$.

Charge stiffness. Similarly, charge stiffness is given by

$$\mathcal{D} = \pi L\frac{\partial^2 E}{\partial \eta^2}$$

which as well is approximated at half filling by

$$\mathcal{D}_{1/2}(L) \equiv \frac{E_g[L, L/2, \delta\eta] + E_g[L, L/2, -\delta\eta] - 2E_g[L, L/2, 0]}{4(\delta\eta)^2} \tag{33}$$

for a "small" flux variation $\delta\eta$. It is important to notice here that the charge compressibility is expected to vanish in gapped phases. The reason is simple: if $\partial_\mu\rho = 0$, that means that shifting infinitesimally the chemical potential does not increase charge density – there is no single-particle state that can accommodate additional particles. Thus, there is a gap. A simple and good signal that a phase has become gapless is the non-vanishing charge compressibility.

3.2 What I actually did

All I described in the above section is a rather good strategy, provided you can simulate a big long chubby chain with a lot of fermions. It turns out, taken into account my computational resources, the entire strategy turns out to be a little optimistic. It would have been wiser to understand my limits earlier, but that's how life goes, I guess. I limited the estimation of the Luttinger parameters u and K to purely qualitative.

3.2.1 Charge gaps

For a model of the class of the spinless Fermi-Hubbard, Eq. (16), the chemical potential part amounts to a pure energy shift when working inside a fixed-number subspace of the many-body Hilbert space. Let $E_g[L, N, \eta]$ be the ground-state energy of Eq. (31) at fixed particle number N. Moreover, let me define

$$\Delta_\rho^{\pm M}[\mu] \equiv E_g[L, \rho L \pm M, \eta] - E_g[L, \rho L, \eta]$$

being $\rho \equiv N/L$ the charge filling and $M \in \mathbb{N}$ a given number of particles (+ sign) or holes (− sign) added as elementary excitations. To diagonalize the model (16) at fixed particles number means that the energy difference must depend on μ/t only by the total number of particles, while on V/t in some complicated unspecified way. This implies

$$\Delta_\rho^{\pm M}[\mu] \equiv f\left(\rho, \frac{V}{t}\right) \mp M\mu \quad \Longrightarrow \quad f\left(\rho, \frac{V}{t}\right) = \Delta_\rho^{\pm M}[\mu] \pm M\mu$$

The parametric dependence of the Δs on μ was specified explicitly. The left-hand side is independent of μ. Let me define $\mu_\rho^\pm$ as the chemical potential at which the gap closes – which is, the set of points on the $[V/t, \mu/t]$ plane where to add particles or holes does not cost energy. Then, computing the above equation's right-hand side at zero chemical potential, it must be

$$\mu_\rho^{\pm M} = \mp \frac{1}{M} \Delta_\rho^{\pm M}[0]$$

Now, recall the notation of Fig. 10: for the half-filling Mott insulating region, $\mathrm{MI}_{1/2}$, the top and bottom borders shall be given by

$$\mu_{1/2}^{\pm 1} = \mp \Delta_{1/2}^{\pm 1}[0] \qquad \text{and} \qquad \mu_{1/2}^{\pm 2} = \mp \frac{1}{2} \Delta_{1/2}^{\pm 2}[0]$$

I reported both the expressions for $M = 1$ and $M = 2$: in our PBC-XXZ general scheme it is formally more correct to perform fixed-N computations preserving the fermion number parity. For the unitary-filling region, MI_1, of course it is not possible to add particles; as expected, just a − phase boundary can be defined at unitary density

$$\mu_1^{-1} = -\Delta_1^{-1}[0] \qquad \text{and} \qquad \mu_1^{-2} = -\frac{1}{2} \Delta_1^{-2}[0]$$

To compute $\Delta_\rho^{\pm M}[\mu]$ is just a matter of computing ground-state energies. This procedure allows for a simple estimation of the phase boundaries and, most importantly, provides insight on the finite-size effects.

A numerical extraction of such phase boundaries was performed for increasing sizes. I used

$$L \in \{14, 22, 30, 38\}$$

in order to maintain an odd particles number at half-filling and keep under control computational runtimes. Moreover, I performed the calculation setting `double` = true – which is, adding or removing two particles – to conserve parity. By direct confrontation of an analogous analysis performed with `double` = false, no significant difference seems to arise. Results are shown in Fig. 12. The MI_1 phase is perfectly coherent with the expectations of Fig. 10, while the same is not true for the $\mathrm{MI}_{1/2}$ phase. Increasing lattice length, however, coherence with expectations seems to improve[7]. An important feature to notice is that, differently from the expectations of Fig. 10, the SU phase is expected to be disconnected (split in two parts). Computationally, finite-size effects could lead to some physical differences in the "upper"-SU and the "lower"-SU phases I analyze briefly in next sections.

Computationally, this analysis had two purposes. First, detect the finite-size phase transition lines positions without running heavy simulations along the entire parameters space. Secondly and most importantly, using these results, one is able to predict the phase where a given point $(V/t, \mu/t)$ is expected to lie. Now, to simulate Mott-insulating systems requires little computational resources given the simplicity of the ground-state: for the Ferromagnetic region the solutions subspace is approximately 1-dimensional, being dominated by the state

$$|11\cdots1\rangle$$

while for the Anti-Ferromagnetic region the subspace is approximately two-dimensional, dominated by the states

$$|0101\cdots01\rangle \qquad |1010\cdots10\rangle$$

[7] A straightforward procedure one should carry out at this point should be one Finite-Size-Scaling to estimate the $L \to \infty$ converged phase-boundaries lines. A procedure of this kind I avoid here, but was analogously carried out by Marco Pompili and me on our previous work.

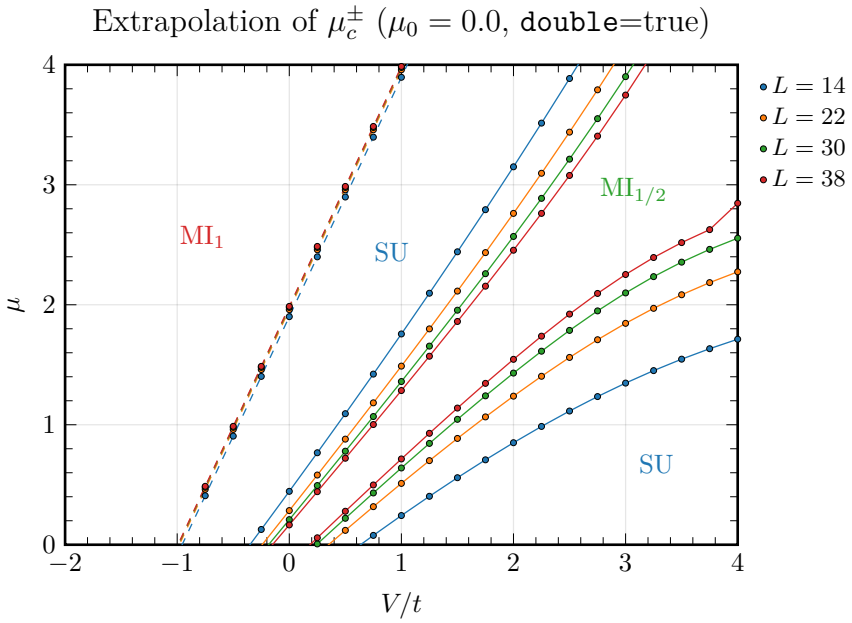

Figure 12 | Estimated position of finite-size chains phase boundaries at increasing lengths. The dashed line on the left delimits the MI$_1$/SU phase transition and represents $\mu_1^{-2}|_{@L}$. The solid lines delimit the MI$_{1/2}$ phase and represent $\mu_{1/2}^{\pm 2}|_{@L}$.

Then, for states expected to be Mott-insulating I have run DMRG algorithms adjusting its simulation parameters to less-expensive configurations without sacrificing accuracy, making use of the rapid convergence times. In DMRG language, I have chosen the following configurations:

```
# Ising Ferromagnet (analog) DMRG parameters

IFnSweeps = 5
IFMaxLinkDim = [10,20,30,40,50]
IFCutoff = [1E-8]

# Ising Anti-Ferromagnet (analog) DMRG parameters

IAFnSweeps = 5
IAFMaxLinkDim = [10,20,30,40,50]
IAFCutoff = [1E-8]

# XY (analog) DMRG paramters

XYnSweeps = 20
XYMaxLinkDim = [10,50,75,200,500]
XYCutoff = [1E-8]
```

Notice that, when the length of the `MaxLinkDim` vector is bigger of the number of sweeps `nSweeps`, the last value of the `MaxLinkDim` vector is used *ad libitum*. For the three phases, the `Cutoff` is set to a generous value and only for the XY phase there is a significant computational difference both in bond-link dimensions and in the number of DMRG sweeps.

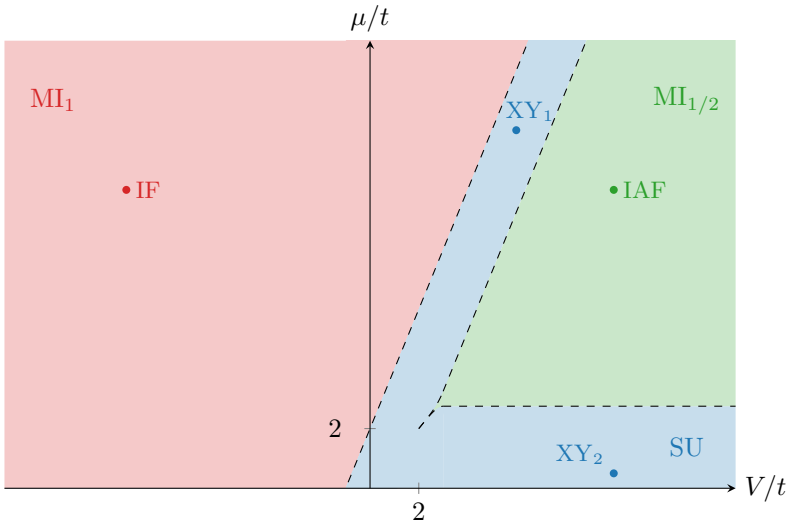

Figure 13 | Plot of the theoretical phase diagram, enlarged from Fig. 10, together with the four simulated points IF $= (-10, 10)$, IAF $= (10, 10)$, $\mathrm{XY}_1 = (6, 12)$ and $\mathrm{XY}_2 = (10, 0.5)$. The points are plotted explicitly with the respective labels; the color refers to the expected phase of the ground-state.

3.2.2 Single-point characterization

A good task is to characterize the three phases by choosing one precise set of parameters representative of each. Each choice $(V/t, \mu/t)$ describes a model whose solution is a given physical phase. The four points I have chosen are:

```
IFPoint  = [-10.0,  10.0]     # MI_1 point
IAFPoint = [ 10.0,  10.0]     # MI_1/2 point
XYPoint1 = [  6.0,  12.0]     # upper SU point
XYPoint2 = [ 10.0,   0.5]     # lower SU point
```

I have explicitly chosen configurations deep in the theoretically expected phases. The points are located on the expected phase diagram in Fig. 13. Various possible analyses can be carried out for single-point simulations. Among others, I decided to analyze the following properties:

1. bipartite entropy of the ground-state,

$$S(\hat{\rho}_\ell) \equiv -\operatorname{Tr}_\ell \{\hat{\rho}_\ell \log \hat{\rho}_\ell\} \tag{34}$$

   as a function of the bipartition length ℓ, being $\hat{\rho}_\ell$ the block reduced density matrix. A sketch of a possible chain bipartition is given in Fig. 14;

2. density variance across a block of sites, defined by

$$\delta n_M^2 = \left\langle \left(\sum_{i \in M} \hat{n}_i \right)^2 \right\rangle - \left\langle \sum_{i \in M} \hat{n}_i \right\rangle^2 \tag{35}$$

   as a function of the block length M. Chain bipartition is carried out as in the previous point[8], with reference to Fig. 14;

3. density-density correlation function as defined in Eq. (14) along sites;

4. superconducting correlation function as defined in Eq. (15) along sites;

[8] We could define block density variance also for non-consecutive site blocks; differently from entropy, sequentiality is not strictly needed but nevertheless implemented.

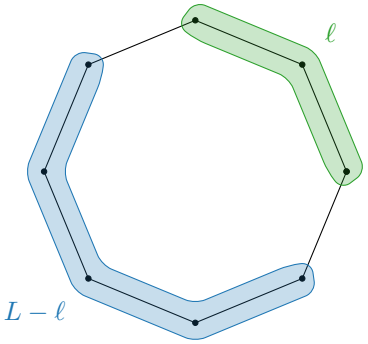

Figure 14 | Illustration of a possible chain bipartition in two parts of lengths ℓ and $L-\ell$, used to calculate Von Neumann entropy across the bipartition bond b (the latter is only defined with respect to the starting site s of the partition, with s being averaged over). I omit b and s labels in plot. Of course, it makes sense to perform bipartition up to $\ell \leq \lfloor L/2 \rfloor$.

The SU states are expected to be significantly more entropic with respect to the Mott insulating states[9]. Similarly, due to increased mobility of fermions as well as entanglement the density variance across sites is expected to be near-zero for the Mott-insulating phase and significantly non-zero for the superconducting phase. Moreover, the above sentence is expected to hold true for the MI_1 phase and approximately true for the $\mathrm{MI}_{1/2}$ phase due to finite-size effects.

Consider Fig. 15: I there sketched the four observables hereby listed computed for $L = 38$, for each of the four points analyzed. For each observable, what is shown is the value averaged along the chain; the error is not shown but can be estimated easily by taking the standard deviation across the chain. As a first comment, as expected bipartite entropy and block density variance are indeed significantly larger on the XY points. Correctly, the $\mathrm{IAF}/\mathrm{MI}_{1/2}$ phase shows both a finite small entropy and a finite small block density variance.

Things get interesting for correlators. Consider the bottom-right plot of Fig. 15, which is, the CDW density-density correlator plot. The red line represents the density-density correlator for the point $\mathrm{IF} = (-10, 10)$ (see Fig. 13). The state is expected to be unitary filled and Mott insulating, which is, well approximated by

$$|\Psi\rangle \simeq |\mathbf{1}\rangle \equiv \bigotimes_{j=1}^{L} \hat{c}_j^\dagger |\Omega\rangle \tag{36}$$

Correctly the density-density correlation function is identically zero. Recalling the power-law behavior of $\mathcal{C}_{\mathrm{CDW}}(r)$ of Eq. (14), such an r-dependence signals $K \to 0$. In the same figure, the green line indicates the simulation at the point $\mathrm{IAF} = (10, 10)$. Define the states:

$$|\mathrm{e}\rangle \equiv \bigotimes_{j=1}^{L/2} \hat{c}_{2j}^\dagger |\Omega\rangle \qquad \text{(even sites filled, odd sites empty)} \tag{37}$$

$$|\mathrm{o}\rangle \equiv \bigotimes_{j=1}^{L/2} \hat{c}_{2j-1}^\dagger |\Omega\rangle \qquad \text{(odd sites filled, even sites filled)} \tag{38}$$

For an half-filled Mott-insulating state, the assumption is that the ground-state is dominated by these two,

$$|\Psi\rangle \simeq \alpha_{\mathrm{e}} |\mathrm{e}\rangle + \alpha_{\mathrm{o}} |\mathrm{o}\rangle + (\cdots) \qquad \alpha_{\mathrm{e}}, \alpha_{\mathrm{o}} \in \mathbb{C} \qquad \sqrt{|\alpha_{\mathrm{e}}|^2 + |\alpha_{\mathrm{o}}|^2} \simeq 1$$

[9] I skip the formal proof of this sentence. Intuitively, this is due to the fact that the Mott-insulating phase is dominated by a small-size Hilbert subspace (1-dimensional for the unitary filling part, 2-dimensional for the half-filling part). Because of this, the unitary-filled phase is exactly separable and the half-filled is low-entangled and almost-separable. In these phases, the ground-state density matrix is sparse. On the contrary, superconducting phase imply heavy entanglement – which is, big entropy – because, being fermion hopping favored, the ground-state density matrix is not sparse at all.

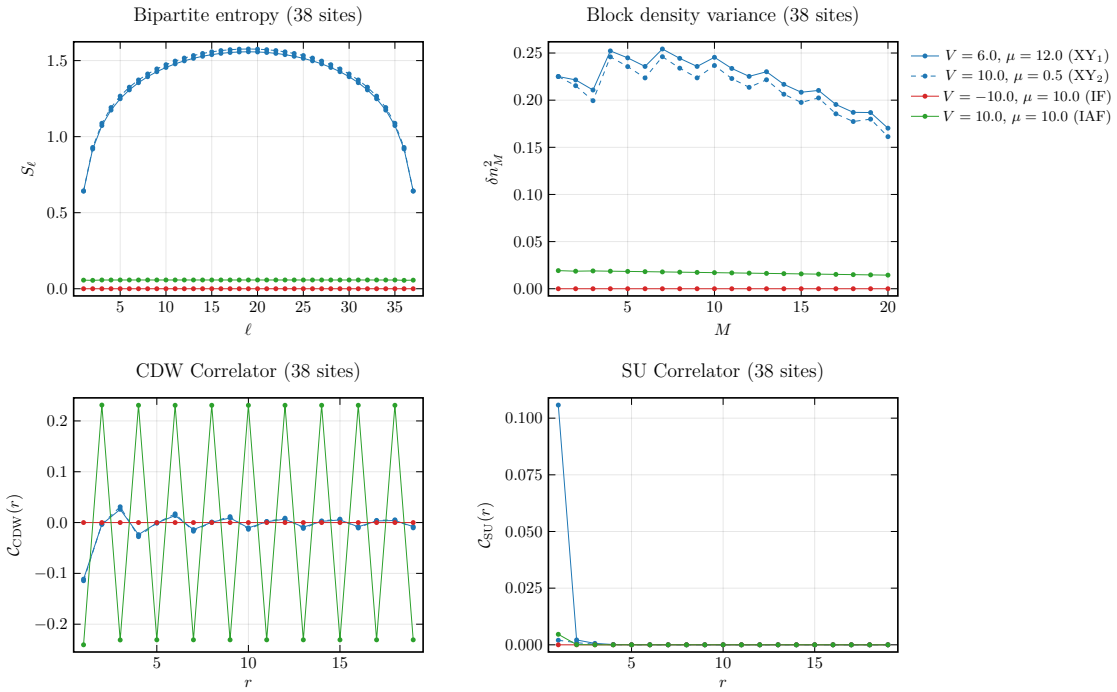

Figure 15 | Compact plot of the four observables listed in Sec. 3.2.2. Top left: bipartite entropy; top right: block density variance; bottom left: density-density correlator; bottom-right: superconducting correlator. The legend on the top left side listing the four analyzed points refers to all figures.

Moreover, the physical expectation is that $|\alpha_{\mathrm{e}}| = |\alpha_{\mathrm{o}}| = 1/2$. For such a situation, is rather easy to show that

$$\langle \delta\hat{\rho}(i)\delta\hat{\rho}(j)\rangle = \frac{1}{2}\left[\langle \mathrm{e}|\hat{\rho}(i)\hat{\rho}(j)|\mathrm{e}\rangle + \langle \mathrm{o}|\hat{\rho}(i)\hat{\rho}(j)|\mathrm{o}\rangle\right] - \frac{1}{4} = \begin{cases} -1/4 & \text{if } |i-j| \text{ is odd} \\ 1/4 & \text{if } |i-j| \text{ is even} \end{cases}$$

an expectation perfectly satisfied by the oscillation visible in Fig. 15, bottom-right panel, green line. Again, recall the expectation of Eq. (14) at half-filling: the correlator oscillation is present, sustained at long distances without suppression – as before, a signal that $K \to 0$.

On the same figure, the dashed and solid blue lines (almost indiscernible) represent the correlator computed for the points $\mathrm{XY}_1 = (6, 12)$ and $\mathrm{XY}_2 = (10, 0.5)$. Two features are visible: the data oscillate on a length scale bigger than the lattice spacing, and the correlator amplitude is suppressed. I have plotted separately the data for the point $\mathrm{XY}_1 = (6, 12)$ in Fig. 16, superimposing a simple Lorentzian computed via the extracted K parameter for this configuration (reported in Figure),

$$-\frac{K}{2\pi^2 r^2}$$

This is the "smooth" part of Eq. (14). The orange line in Fig.16 is not a fit, is just intended as an illustration. To get more quantitative, one could fit the found data with a three-parameters model from Eq. (14). Without any good estimation for α, I could not do anything more.

Finally, on the bottom right panel of Fig. 15 I have reported the simulated data for $\mathcal{C}_{\mathrm{SU}}(r)$. For what is intelligible in the plot, coherently with expectations, the Mott-insulating states' correlators vanish identically. For the sake of intelligibility, I also plotted the XY data on a `:loglog` scale in Fig. 17. For both the points simulated, the decay is vaguely power-law with some evident deviations at big distance. I reconnect this last effect to the finite size: the finite nature of the chain introduces another length scale over which correlations decay, related directly to L. Over this length scale decay is expected to be exponential-like. Regarding Fig. 17, there is nothing much I can say apart from *much* qualitative comments. I tried comparing with a power-law decay using

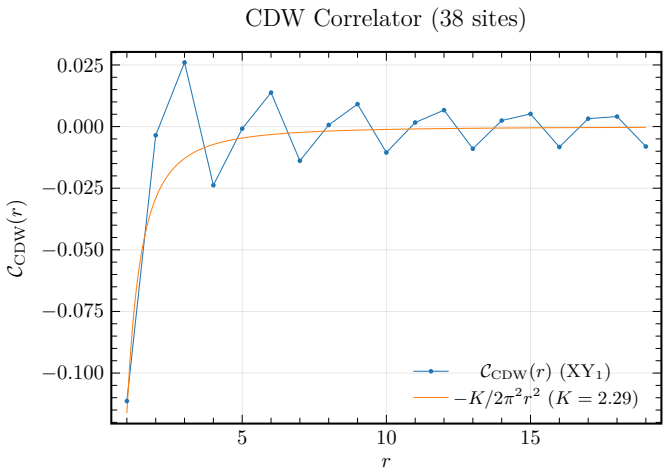

Figure 16 | Plot of $\mathcal{C}_{\mathrm{CDW}}(r)$ limited to the data of the simulation at point $\mathrm{XY}_1 = (6, 12)$. Superimposed to the plot, I have plotted a simple Lorentzian decay function with estimated strength K. This is not a fit whatsoever.

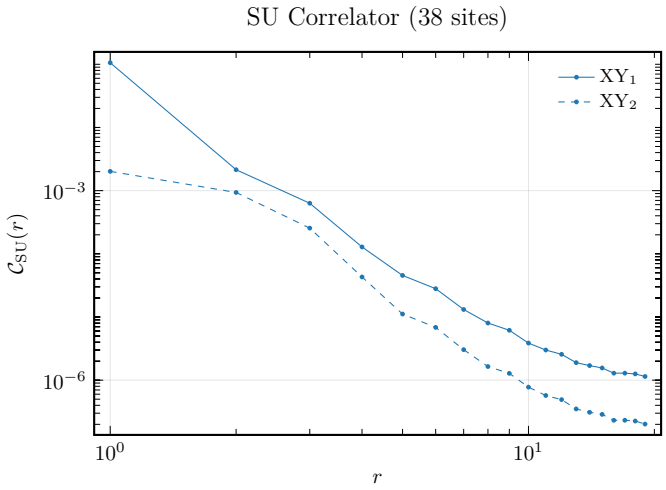

Figure 17 | Logarithmic plot of $\mathcal{C}_{\mathrm{SU}}(r)$. The power-law decay is qualitatively visible and would require deeper and quantitative investigation.

the estimated K, as in Fig. 16, but results were unsatisfying. Evidently the simulations are not good enough to represent these correlations.

3.2.3 Observables heatmaps

In this last section I sketch some relevant observables heatmaps. Results are described qualitatively but give space to deep understanding of how the (finite-size) phases are made.

Density. I start by commenting the results shown in Fig. 18. The first and simplest observable is the average particle density along the chain, shown as a heatmap in Fig. 18a. As expected the left-side IF/MI$_1$ phase is unitary filled, while the expected IAF/MI$_{1/2}$ is almost uniformly half-filled. Due to finite size, which implies finite particle number, in the expected XY phase uniform-density domains borders are clearly visible. These correspond to single particles removal.

Interestingly, at zero chemical potential (no system-environment matter exchange) the expected density at strong NN repulsion is less than half. To alternate particles and holes in not enough to

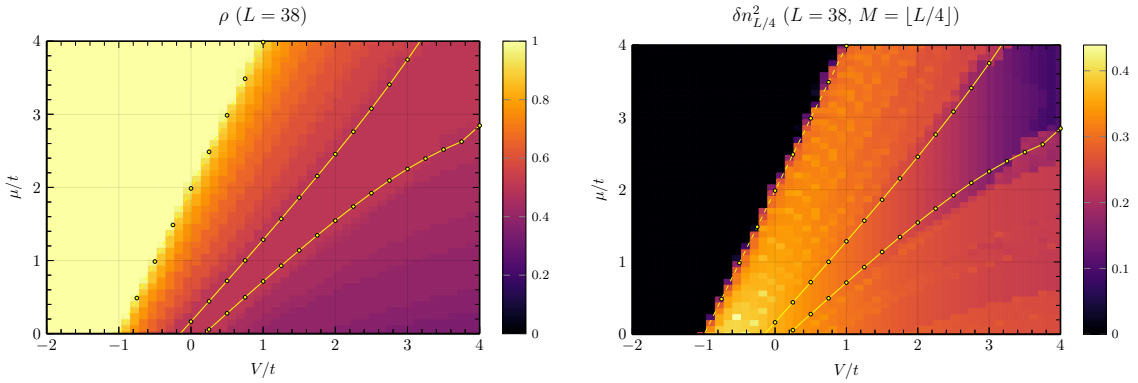

a | Density heatmap.

b | Block density variance heatmap.

Figure 18 | The averaged density heatmap for the DMRG solved ground state of the spinless Fermi-Hubbard model is shown in Fig 18a. Superimposed and with the same criteria as in Fig. 12 are the expected phase boundaries. Fig. 18b depicts the average density variance across a block of sites of length $M = \lfloor L/4 \rfloor$.

gain energy: residual subdominant hopping makes the ground state converge onto a less populated state.

Block density variance. Fig. 18b shows the block density variance $\langle \delta \hat{n}^2_M \rangle$ as a heatmap for $M = \lfloor L/4 \rfloor$. For the IF/MI$_1$ phase, the variance of density along the block is null – a consequence of the robust ground-state $|\Psi\rangle \simeq |\mathbf{1}\rangle$ as defined in Eq. (36). Similarly, the dominant contribution to the IAF/MI$_{1/2}$ phase is given by the states $|\mathrm{e}\rangle$ and $|\mathrm{o}\rangle$ as defined respectively in Eqns. (37), (38). Separately, each of these states is a number operator eigenstate and thus has zero density variance on each site and on every block. For a state in Span$\{|\mathrm{e}\rangle, |\mathrm{o}\rangle\}$ the variance over a block is expected to be small:

$$|\Psi\rangle = \frac{1}{\sqrt{1+|\gamma|^2}} |\mathrm{e}\rangle + \frac{\gamma}{\sqrt{1+|\gamma|^2}} |\mathrm{o}\rangle \qquad \gamma \in \mathbb{C}$$

and

$$\langle \Psi | \hat{n}_j | \Psi \rangle = \frac{1+(-1)^j}{2} \frac{1}{1+|\gamma|^2} + \frac{1-(-1)^j}{2} \frac{|\gamma|^2}{1+|\gamma|^2} = \langle \Psi | \hat{n}_j^2 | \Psi \rangle$$

Since

$$\left(\frac{1 \pm (-1)^j}{2} \right)^2 = \frac{1 \pm (-1)^j}{2} \qquad \text{and} \qquad \frac{1 \pm (-1)^j}{2} \frac{1 \mp (-1)^j}{2} = 0$$

this implies using some basic algebra

$$\langle \Psi | \hat{n}_j^2 | \Psi \rangle - \langle \Psi | \hat{n}_j | \Psi \rangle^2 = \frac{|\gamma|^2}{\left(1+|\gamma|^2\right)^2} \leq \frac{1}{4}$$

the last inequality being trivial to prove and satisfied $\forall \gamma \in \mathbb{C}$. One can show easily that if the state is not dominated by $|\mathrm{e}\rangle, |\mathrm{o}\rangle$ and the number of particles on the chain is allowed to fluctuate – as is in the superpositions composing the XY ground states – the j-site variance increases. Such difference becomes even sharper when considering a block of sites of length M instead of a single site j[10]. In Fig. 18b such a behavior is observed, becoming more and more important as we approach the top-right side of the picture, coherently with the theoretical expectations of Fig. 10. This last property

[10] I will not show this here, being the proof purely algebraic and not so interesting. This behavior essentially arises because of the appearance of connected density-density correlation functions, whose power-law decay in XY phase produces the "boost" of the observable.

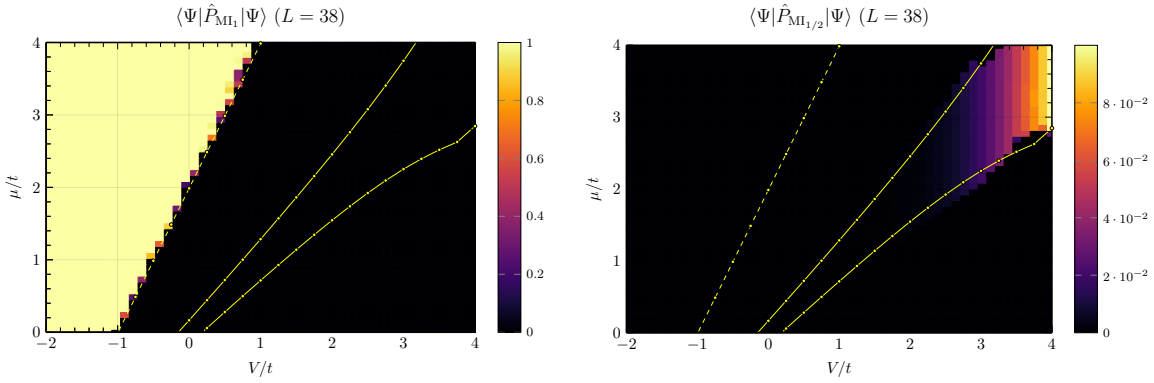

a | Overlap with $|\mathbf{1}\rangle$.

b | Overlap with Span$\{|\mathrm{e}\rangle, |\mathrm{o}\rangle\}$.

Figure 19 | In Fig. 19a the projection of the ground-state onto the pure IF/MI$_1$ subspace is shown; such subspace is spanned by $|\mathbf{1}\rangle \equiv |11\cdots1\rangle$. Similarly, Fig. 19b shows the projection of the ground-state onto the pure IAF/MI$_{1/2}$ subspace, given by Span$\{|\mathrm{e}\rangle, |\mathrm{o}\rangle\}$.

is interesting, because it signals that the finite-size version of the gapped IAF/MI$_{1/2}$ phase extends over a broad region but remains most similar to its thermodynamic limit in the correct part of the phase diagram.

Projection onto Mott subspaces. A good confirmation of the assumptions of the above paragraph is to check directly how much the ground-state is projected onto a given Mott subspace. Let me start by the IF/MI$_1$ phase. Let me define

$$\hat{\mathrm{P}}_{\mathrm{MI}_1} = |\mathbf{1}\rangle\langle\mathbf{1}|$$

Evidently, if

$$|\Psi\rangle = \alpha_{\mathbf{1}}\,|\mathbf{1}\rangle + \sum_{\psi} \alpha_{\psi}\,|\psi\rangle$$

being $|\psi\rangle$ any other state and the αs the amplitudes, we get

$$\left\langle \hat{\mathrm{P}}_{\mathrm{MI}_1} \right\rangle = |\alpha_{\mathbf{1}}|^2$$

which is the probability for the state to coincide (up to an irrelevant phase) with $|\mathbf{1}\rangle$. Consider Fig. 19a: inside the expected IF/MI$_1$ region, the convergence of the simulated state on $|\mathbf{1}\rangle$ is absolute. Outside, the simulated state is (obviously) orthogonal to $|\mathbf{1}\rangle$. I defined this MPO simply as

```
function GetUnitaryMIProjector(
        sites::Any
    )::MPO

    L = length(sites)

    states = ["1" for j in 1:L]      # 1111...
    u = MPS(sites, states)           # Unitary-filled state

    UP = projector(u)
    return UP

end
```

$\langle \hat{\mathrm{P}}_{\mathrm{MI}_{1/2}} \rangle \Big\vert_{L,V/t,\mu/t}$				
	$V/t = \mu/t$			
L	5	10	20	50
38	0.238	0.692	0.912	0.985
54	0.127	0.591	0.876	0.979
70	0.068	0.504	0.842	0.973
86	0.036	0.43	0.809	0.967
102	0.019	0.366	0.777	0.96
118	0.01	0.312	0.747	0.954
134	0.006	0.266	0.717	0.948
150	0.003	0.227	0.689	0.942

Table 2 | Probability for the simulated ground state of the model with $V/t = \mu/t$ as specified in the first row to be in the subspace $\mathrm{Span}\{|\mathrm{e}\rangle, |\mathrm{o}\rangle\}$ at increasing chain lengths L.

Similarly, let me define

$$\hat{\mathrm{P}}_{\mathrm{MI}_{1/2}} = |\mathrm{e}\rangle\langle\mathrm{e}| + |\mathrm{o}\rangle\langle\mathrm{o}|$$

the projector onto the IAF/$\mathrm{MI}_{1/2}$ phase. With analogous notation as above,

$$\left\langle \hat{\mathrm{P}}_{\mathrm{MI}_{1/2}} \right\rangle = |\alpha_{\mathrm{e}}|^2 + |\alpha_{\mathrm{o}}|^2$$

which is the probability for the ground-state of being in the $\mathrm{Span}\{|\mathrm{e}\rangle, |\mathrm{o}\rangle\}$ subspace. The MPO was initialized as:

```
function GetHalfMIProjector(
        sites::Any
    )::MPO

    L = length(sites)

    states = [isodd(j) ? "0" : "1" for j in 1:L] # 0101...
    e = MPS(sites, states)                       # Even-filled state

    states = [isodd(j) ? "1" : "0" for j in 1:L] # 1010...
    o = MPS(sites, states)                       # Odd-filled state

    E = projector(e) # Normalized projector
    O = projector(o) # Normalized projector
    HP = E+O
    return HP

end
```

Now, I expected the projection probability to saturate quickly to unity with better and better approximation as the chain got larger. Instead, as is visible in Fig. 19b, it turns out that the simulated state lies in the $\mathrm{Span}\{|\mathrm{e}\rangle, |\mathrm{o}\rangle\}$ subspace with a probability of approximately 10%. Correctly, the projection probability seems to increase by moving to the top-right corner. Of course I expected way better results. I tried changing the DMRG parameters (specifically `nSweeps`) but noticed no measurable improvement: the algorithm converges quickly. I tried simulating different $(V/t, \mu/t)$ choices at increasing lattice dimension.

Consider Tab. 2: there are reported the results of the expectation value of the projector over ground states simulated at increasing ratios $V/t = \mu/t$ – which is, on the top-right diagonal. The last column (calculated in the extreme anti-ferromagnetic parametrization), correctly, saturates

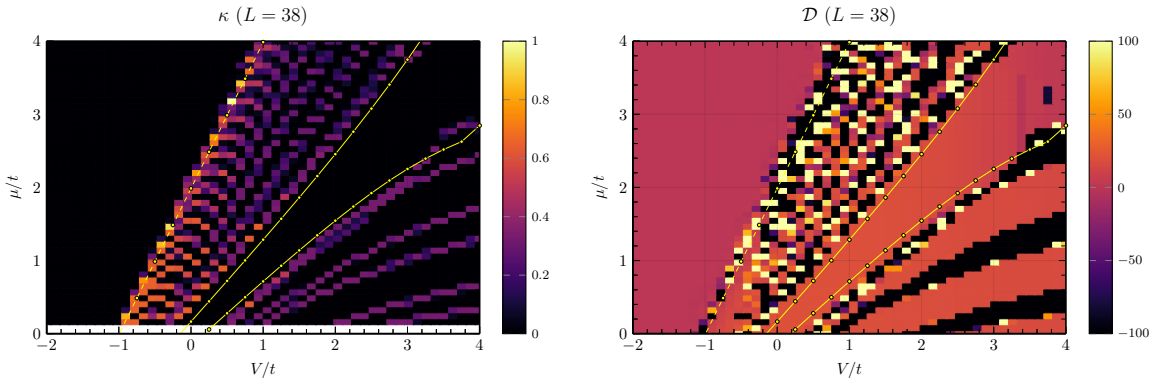

a | Charge compressibility.

b | Charge stiffness.

Figure 20 | In Fig. 20a, the ground state compressibility is reported. The low part of the plot (small chemical potential) has been omitted: compressibility was here computed by the means of finite differences, a technique requiring cached data from previous simulations. Finite differentiation is also responsible for the smearing of the heatmap across the phase boundaries. In Fig 20b the charge stiffness for a small flux threading the chain is plotted.

at almost unity. Lowering the parameters and increasing the lattice length, interestingly the probability decreases down to extremely small values (below 1% for $L > 118$, $V/t = \mu/t = 5$). I have tried using more generous DMRG parameters, but results did not improve much. Probably, these data are explained by the fact that – even if algebraically simple – the IAF ground state is non-locally entangled. This means, even if the number of many-body states entangled is low, in the physical ground state in thermodynamic limit each site is entangled with every other – a condition of low long-range entanglement Finite-Size DMRG struggles to reproduce over finite lengths. Probably the simulated states is more similar to a collection of cluster of sites entangled Anti-Ferromagnetically.

A possible measurement one could carry out (I did not) is the averaged projection onto finite-size Anti-Ferromagnetic local projectors,

$$\hat{\mathrm{P}}^{M}_{\mathrm{MI}_{1/2}} = \frac{1}{L}\sum_{s=1}^{L}\left[\bigotimes_{j=s}^{s+M}\hat{c}^{\dagger}_{2j}\,|\Omega\rangle\langle\Omega|\bigotimes_{k=s}^{s+M}\hat{c}_{2k} + \bigotimes_{j=s}^{s+M}\hat{c}^{\dagger}_{2j-1}\,|\Omega\rangle\langle\Omega|\bigotimes_{k=s}^{s+M}\hat{c}_{2k-1}\right]$$

which is, the equivalent of the projector analyzed above but limited to blocks of length M and averaged over different blocks.

Luttinger parameters. Finally, I explored roughly the behavior of charge compressibility κ and charge stiffness $\mathcal{D}$, as explained in Sec. 3.1. Both observables are extracted by the means of finite derivatives: κ, by looking at the density difference at two close chemical potentials; $\mathcal{D}$, by looking at the current response to small fluxes, which is, the energy derivative response.

Fig. 20a shows a heatmap of the finite-size compressibility. Taking into account the roughness of the simulation, coherence with the expectations is acceptable. The two interesting Mott-insulating regions are almost uniformly non compressible, a signature of the presence of a gap. Outside, fluctuations in compressibility are visible. It must be noted that, for an infinitely long chain (the continuum limit) the step-like regions of gradually decreasing density of Fig. 18a between the two Mott phases degenerate into a continuum. In other words: moving from the unitary-filled to the half-filled region, the density varies continuously. For a small finite chain, the finite-size effect is the step-like variation of density, a feature giving rise to the aforementioned fringes as well as the zero-compressibility regions in the bottom right corner of the phase diagram 20a. These regions are not generated by a thermodynamically gapped phase, rater by the finite-size nature of the simulation.

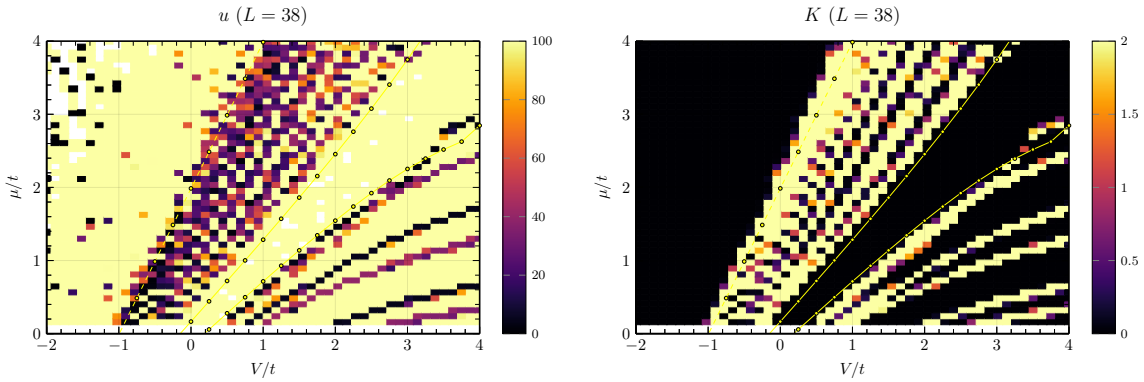

a | u Luttinger paramter.

b | K Luttinger parameter.

Figure 21 | Honestly, I have no idea what is going on in Fig. 21a, showing the renormalized velocity u. In order to make the data intelligible I had to apply a cutoff of 100. In Fig. 21b the heatmap for the Luttinger parameter K is sketched. The low part has been cut off because of the finite-differences method used to compute κ.

In Fig. 20b the charge stiffness heatmap is reported. Similar observations as for the charge compressibility hold for $\mathcal{D}$. The IF/MI$_1$ phase is stiff: given some flux threading the chain, static Mott-localization gives null current response. A non-zero current response requires the possibility of hopping, which in turn requires a filled site near an empty site. No infinitesimal flux can be responsible of the global synchronized rotation of all the fermions in the unitary-filled state. The IAF/MI$_{1/2}$ presents a small finite positive stiffness, gradually decreasing to zero in the top-right corner of Fig. 20b. Analogous considerations as for the unitary filled state hold here, and Mott localization explains the stiffness. Outside, as for κ, fringes are visible. Interestingly, changes in parity appear to cause current response to diverge negatively.

Recall now Eqns. (30),

$$u = \sqrt{\frac{\mathcal{D}}{\pi\kappa}} \qquad \text{and} \qquad K = \sqrt{\pi\kappa\mathcal{D}}$$

Compressibility and charge stiffness, multiplied and divided, are connected to the Luttinger parameters u and K. The two parameters completely govern the bosonization description of a one-dimensional spinless fermionic system. Most importantly, as explained in Sec. 1.3.3, if $K < 1$ the equivalent interaction between bosons is repulsive and gives rise to a CDW behavior. If $K > 1$, the interaction is attractive and the main dynamics is superfluid.

Comically, the u and K heatmaps of Fig. 21 – which should have been the entire point of this whole project – are not so satisfying. On one hand, the plot for u in Fig. 21a – apart from the general structure – is not insightful, oscillates strangely in the robust ferromagnetic phase and is evidently suffering from some numerical error in calculating u starting from κ, $\mathcal{D}$. On the other hand Fig. 21b shows – as expected – a strongly suppressed K in the Mott-insulating region (signaling a CDW kind of order), while outside the same parameter oscillates and reaches values much bigger than 1. Note that the heatmap has been limited to the values $[0, 2]$ for intelligibility reasons. Apart from this consideration, which confirms expectations, not much more can be said.

Let me close with a positive note. At least, the heatmap for the Luttinger parameter K in Fig. 21b makes sense in the bosonization framework. Remembering the many turns of this project, I could not have asked for more.

That's all folks!

References

[1] Jan von Delft and Herbert Schoeller. "Bosonization for beginners — refermionization for experts". In: *Annalen der Physik* 510.4 (1998), pp. 225–305. DOI: https://doi.org/10.

1002/andp.19985100401. eprint: https://onlinelibrary.wiley.com/doi/pdf/10.1002/andp.19985100401. URL: https://onlinelibrary.wiley.com/doi/abs/10.1002/andp.19985100401.

[2] Fabio Franchini. *An Introduction to Integrable Techniques for One-Dimensional Quantum Systems*. Vol. 940. Sept. 2016. ISBN: 9783319484860. DOI: 10.1007/978-3-319-48487-7.

[3] Thierry Giamarchi. *Quantum Physics in One Dimension*. Oxford University Press, Dec. 2003. ISBN: 9780198525004. DOI: 10.1093/acprof:oso/9780198525004.001.0001. URL: https://doi.org/10.1093/acprof:oso/9780198525004.001.0001.

[4] F D M Haldane. "'Luttinger liquid theory' of one-dimensional quantum fluids. I. Properties of the Luttinger model and their extension to the general 1D interacting spinless Fermi gas". In: *Journal of Physics C: Solid State Physics* 14.19 (July 1981), p. 2585. DOI: 10.1088/0022-3719/14/19/010. URL: https://dx.doi.org/10.1088/0022-3719/14/19/010.

[5] E. Miranda. "Introduction to bosonization". In: *Brazilian Journal of Physics* 33.1 (Mar. 2003), pp. 3–35. ISSN: 0103-9733. DOI: 10.1590/S0103-97332003000100002. URL: https://doi.org/10.1590/S0103-97332003000100002.

[6] Mykhailo V. Rakov, Michael Weyrauch, and Briiissuurs Braiorr-Orrs. "Symmetries and entanglement in the one-dimensional spin-$\frac{1}{2}$ XXZ model". In: *Phys. Rev. B* 93 (5 Feb. 2016), p. 054417. DOI: 10.1103/PhysRevB.93.054417. URL: https://link.aps.org/doi/10.1103/PhysRevB.93.054417.

[7] David Senechal. "An Introduction to bosonization". In: *CRM Workshop on Theoretical Methods for Strongly Correlated Fermions*. Aug. 1999. arXiv: cond-mat/9908262.

[8] Jesko Sirker and Michael Bortz. "The open XXZ-chain: bosonization, the Bethe ansatz and logarithmic corrections". In: *Journal of Statistical Mechanics: Theory and Experiment* 2006.01 (Jan. 2006), P01007. DOI: 10.1088/1742-5468/2006/01/P01007. URL: https://dx.doi.org/10.1088/1742-5468/2006/01/P01007.